Z. Phys. C - Particles and Fields 55, 191–207 (1992)

Zeitschrift für Physik C Particles and Fields

A measurement of electron production in hadronic Z^0 decays and a determination of $\Gamma(Z^0 \to b\bar{b})$

OPAL Collaboration

P.D. Acton[25], G. Alexander[23], J. Allison[16], P.P. Allport[5], K.J. Anderson[9], S. Arcelli[2], P. Ashton[16], A. Astbury[28], D. Axen[29], G. Azuelos[18,a], G.A. Bahan[16], J.T.M. Baines[16], A.H. Ball[17], J. Banks[16], G.J. Barker[13], R.J. Barlow[16], J.R. Batley[5], G. Beaudoin[18], A. Beck[23], J. Becker[10], T. Behnke[27], K.W. Bell[20], G. Bella[23], P. Berlich[10], S. Bethke[11], O. Biebel[3], U. Binder[10], I.J. Bloodworth[1], P. Bock[11], B. Boden[3], H.M. Bosch[11], S. Bougerolle[29], B.B. Brabson[12], H. Breuker[8], R.M. Brown[20], R. Brun[8], A. Buijs[8], H.J. Burckhart[8], P. Capiluppi[2], R.K. Carnegie[6], A.A. Carter[13], J.R. Carter[5], C.Y. Chang[17], D.G. Charlton[8], P.E.L. Clarke[25], I. Cohen[23], W.J. Collins[5], J.E. Conboy[15], M. Cooper[22], M. Couch[1], M. Coupland[14], M. Cuffiani[2], S. Dado[22], G.M. Dallavalle[2], S. De Jong[8], P. Debu[21], L.A. del Pozo[5], M.M. Deninno[2], A. Dieckmann[11], M. Dittmar[4], M.S. Dixit[7], E. do Conto el Silva[12], E. Duchovni[26], G. Duckeck[11], I.P. Duerdoth[16], D.J.P. Dumas[6], P.A. Elcombe[5], P.G. Estabrooks[6], E. Etzion[23], H.G. Evans[9], F. Fabbri[2], M. Fincke-Keeler[28], H.M. Fischer[3], D.G. Fong[17], C. Fukunaga[24,b], A. Gaidot[21], O. Ganel[26], J.W. Gary[4], J. Gascon[18], R.F. McGowan[16], N.I. Geddes[20], C. Geich-Gimbel[3], S.W. Gensler[9], F.X. Gentit[21], G. Giacomelli[2], V. Gibson[5], W.R. Gibson[13], J.D. Gillies[20], J. Goldberg[22], M.J. Goodrick[5], W. Gorn[4], C. Grandi[2], F.C. Grant[5], J. Hagemann[27], G.G. Hanson[12], M. Hansroul[8], C.K. Hargrove[7], P.F. Harrison[13], J. Hart[5], P.M. Hattersley[1], M. Hauschild[8], C.M. Hawkes[8], E. Heflin[4], R.J. Hemingway[6], R.D. Heuer[8], J.C. Hill[5], S.J. Hillier[1], D.A. Hinshaw[18], C. Ho[4], J.D. Hobbs[8], P.R.Hobson[25], D. Hochman[26], R.J. Homer[1], A.K. Honma[28,a], S.R. Hou[17], C.P. Howarth[15], R.E. Hughes-Jones[16], R. Humbert[10], P. Igo-Kemenes[11], H. Ihssen[11], D.C. Imrie[25], A.C. Janissen[6], A. Jawahery[17], P.W. Jeffreys[20], H. Jeremie[18], M. Jimack[2], M. Jobes[1], R.W.L. Jones[13], P. Jovanovic[1], D. Karlen[6], K. Kawagoe[24], T. Kawamoto[24], R.K. Keeler[28], R.G. Kellogg[17], B.W. Kennedy[15], D.E. Klem[19], T. Kobayashi[24], T.P. Kokott[3], S. Komamiya[24], L. Köpke[8], J.F. Kral[8], R. Kowalewski[6], H. Kreutzmann[3], J. von Krogh[11], J. Kroll[9], M. Kuwano[24], P. Kyberd[13], G.D. Lafferty[16], F. Lamarche[18], W.J. Larson[4], J.G. Layter[4], P. Le Du[21], P. Leblanc[18], A.M. Lee[17], M.H. Lehto[15], D. Lellouch[26], P. Lennert[11], C. Leroy[18], J. Letts[4], S. Levegrün[3], L. Levinson[26], S.L. Lloyd[13], F.K. Loebinger[16], J.M. Lorah[17], B. Lorazo[18], M.J. Losty[7], X.C. Lou[12], J. Ludwig[10], M. Mannelli[8], S. Marcellini[2], G. Maringer[3], A.J. Martin[13], J.P. Martin[18], T. Mashimo[24], P. Mättig[3], U. Maur[3], J. McKenna[28], T.J. McMahon[1], J.R. McNutt[25], F. Meijers[8], D. Menszner[11], F.S. Merritt[9], H. Mes[7], A. Michelini[8], R.P. Middleton[20], G. Mikenberg[26], J. Mildenberger[6], D.J. Miller[15], R. Mir[12], W. Mohr[10], C. Moisan[18], A. Montanari[2], T. Mori[24], M.W. Moss[16], T. Mouthuy[12,c], B. Nellen[3], H.H. Nguyen[9], S.W. O'Neale[8,d], B.P. O'Neill[4], F.G. Oakham[7], F. Odirici[2], M. Ogg[6], H.O. Ogren[12], H. Oh[4], C.J. Oram[28,a], M.J. Oreglia[9], S. Orito[24], J.P. Pansart[21], B. Panzer-Steindel[8], P. Paschievici[26], G.N. Patrick[20], S.J. Pawley[16], P. Pfister[10], J.E. Pilcher[9], D. Pitman[28], D.E. Plane[8], P. Poffenberger[28], B. Poli[2], A. Pouladdej[6], E. Prebys[8], T.W. Pritchard[13], H. Przysiezniak[18], G. Quast[27], M.W. Redmond[9], D.L. Rees[1], K. Riles[4], S.A. Robins[13], D. Robinson[8], A. Rollnik[3], J.M. Roney[9], E. Ros[8], S. Rossberg[10], A.M. Rossi[2,e], M. Rosvick[28], P. Routenburg[6], K. Runge[10], O. Runolfsson[8], D.R. Rust[12], S. Sanghera[6], M. Sasaki[24], A.D. Schaile[10], O. Schaile[10], W. Schappert[6], P. Scharff-Hansen[8], P. Schenk[28], H. von der Schmitt[11], S. Schreiber[3], J. Schwiening[3], W.G. Scott[20], M. Settles[12], B.C. Shen[4], P. Sherwood[15], R. Shypit[29], A. Simon[3], P. Singh[13], G.P. Siroli[2], A. Skuja[17], A.M. Smith[8], T.J. Smith[8], G.A. Snow[17], R. Sobie[28,f], R.W. Springer[17], M. Sproston[20], K. Stephens[16], R. Ströhmer[11], D. Strom[9,g], H. Takeda[24], T. Takeshita[24,h], P. Taras[18], S. Tarem[26], P. Teixeira-Dias[11], N.J. Thackray[1], G. Transtromer[25], T. Tsukamoto[24], M.F. Turner[5], G. Tysarczyk-Niemeyer[11], D. Van den plas[18], R. Van Kooten[8], G.J. VanDalen[4], G. Vasseur[21], C.J. Virtue[19], A. Wagner[27], D.L. Wagner[9], C. Wahl[10], J.P. Walker[1], C.P. Ward[5], D.R. Ward[5], P.M. Watkins[1], A.T. Watson[1], N.K. Watson[8], M. Weber[11], P. Weber[6], S. Weisz[8], P.S. Wells[8], N. Wermes[11], M.A. Whalley[1], G.W. Wilson[21], J.A. Wilson[1], I. Wingerter[8], V.-H. Winterer[10], T. Wlodek[26], N.C. Wood[16], S. Wotton[11], T.R. Wyatt[16], R. Yaari[26], Y. Yang[4,i], G. Yekutieli[26], M. Yurko[18], W. Zeuner[8], G.T. Zorn[17]

[1] School of Physics and Space Research, University of Birmingham, Birmingham, B15 2TT, UK
[2] Dipartimento di Fisica dell'Università di Bologna and INFN, Bologna, 40126, Italy
[3] Physikalisches Institut, Universität Bonn, W-5300 Bonn 1, Federal Republic of Germany
[4] Department of Physics, University of California, Riverside, CA 92521, USA
[5] Cavendish Laboratory, Cambridge, CB3 0HE, UK
[6] Carleton University, Department of Physics, Colonel By Drive, Ottawa, Ontario K1S 5B6, Canada
[7] Centre for Research in Particle Physics, Carleton University, Ottawa, Ontario K1S 5B6, Canada
[8] CERN, European Organisation for Particle Physics, 1211 Geneva 23, Switzerland
[9] Enrico Fermi Institute and Department of Physics, University of Chicago, Chicago IL 60637, USA

[10] Fakultät für Physik, Albert Ludwigs Universität, W-7800 Freiburg, Federal Republic of Germany
[11] Physikalisches Institut, Universität Heidelberg, W-6900 Heidelberg, Federal Republic of Germany
[12] Indiana University, Department of Physics, Swain Hall West 117, Bloomington, IN 47405, USA
[13] Queen Mary and Westfield College, University of London, London, E1 4NS, UK
[14] Birkbeck College, London, WC1E 7HV, UK
[15] University College London, London, WC1E 6BT,UK
[16] Department of Physics, Schuster Laboratory, The University, Manchester, M13 9PL, UK
[17] Department of Physics and Astronomy, University of Maryland, College Park, MD 20742, USA
[18] Laboratoire de Physique Nucléaire, Université de Montréal, Montréal, Quebec, H3C 3J7, Canada
[19] National Research Council of Canada, Herzberg Institute of Astrophysics, Ottawa, Ontario K1A 0R6, Canada
[20] Rutherford Appleton Laboratory, Chilton, Didcot, Oxfordshire, OX11 0QX, UK
[21] DPhPE, CEN Saclay, F-91191 Gif-sur-Yvette, France
[22] Department of Physics, Technion-Israel Institute of Technology, Haifa 32000, Israel
[23] Department of Physics and Astronomy, Tel Aviv University, Tel Aviv 69978, Israel
[24] International Centre for Elementary Particle Physics and Department of Physics, University of Tokyo, Tokyo 113, and Kobe University, Kobe 657, Japan
[25] Brunel University, Uxbridge, Middlesex, UB8 3PH, UK
[26] Nuclear Physics Department, Weizmann Institute of Science, Rehovot, 76100, Israel
[27] Universität Hamburg/DESY, II Institut für Experimentalphysik, W-2000 Hamburg 52, Federal Republic of Germany
[28] University of Victoria, Department of Physics, PO Box 3055, Victoria BC V8W 3P6, Canada
[29] University of British Columbia, Department of Physics, 6224 Agriculture Road, Vancouver BC V6T 1Z1, Canada

Received 13 March 1992

Abstract. The production rate of electrons with momentum $p > 4$ GeV/c and large momentum transverse to the jet containing the electron has been measured in 136 000 hadronic decays of the Z^0 recorded with the OPAL detector at LEP in 1990. The dominant source of these electrons is the semileptonic decay of hadrons containing b quarks. If we assume that the semileptonic branching fraction of b hadrons produced on the Z^0 resonance is the same as the branching fraction measured at the $\Upsilon(4S)$ resonance, we determine $\Gamma_{b\bar{b}} = 394 \pm 13 \pm 32$ MeV, where the first error is statistical and the second error is systematic. The sensitivity of the result to this assumption is discussed. We have reduced the dependence of our result on the model of b hadron semileptonic decay by taking into account the correlation between the model dependence of the branching fractions measured at the $\Upsilon(4S)$ and of our kinematic acceptance for electrons.

1 Introduction

The measurement of the partial widths of the Z^0 to quarks and leptons allows a fundamental test of Standard Model of electroweak interactions. The OPAL collaboration has measured the leptonic and hadronic widths of the Z^0 to a precision of 1%, and the measured values [1] are in good agreement with theoretical predictions. The test of the theory is incomplete without the measurement of the partial widths of the Z^0 to individual quark flavours. The measurement of the partial width to b quarks, $\Gamma_{b\bar{b}}$, is of particular interest, because there are electroweak vertex corrections involving t quarks that are uniquely large for the b quark [2]. These large vertex corrections partially cancel the effect of loop diagrams with t quarks, so that the theoretical prediction of $\Gamma_{b\bar{b}}$ has very little dependence on the mass of the top quark. A measurement of $\Gamma_{b\bar{b}}$ to 1% precision would allow a test of these electroweak corrections. Extensions of the Standard Model with mixing between ordinary and exotic fermions predict shifts [3, 4] in $\Gamma_{b\bar{b}}$ from the Standard Model value.

Leptons are a well established signature of the decay of b-flavoured and c-flavoured hadrons. Several measurements of heavy quark production cross sections in e^+e^- collisions using leptons to tag heavy quark decays have been reported [5–8] at centre-of-mass energies $\sqrt{s} \approx M_Z$, where M_Z is the mass of the Z^0. Other methods to determine $\Gamma_{b\bar{b}}$ have also been used [9, 10]. The previously published OPAL measurement of heavy quark production [8] is based on muon production in hadronic Z^0 decays. This paper reports a determination of $\Gamma_{b\bar{b}}$ using electrons with momentum $p > 4$ GeV/c.

Electrons in this momentum range are expected to come from*

- primary b-flavoured hadron decays, $b \to e^- \bar{\nu}_e X$;
- the secondary decay products of b-flavoured hadrons, $b \to c \to e^+ \nu_e X$, $b \to \bar{c} \to e^- \bar{\nu}_e X$, $b \to \tau^- \to e^- \bar{\nu}_e X$, and $b \to \psi \to e^+ e^- X$;
- the direct production of charmed hadrons, $Z^0 \to c\bar{c}$, with $c \to e^+ \nu_e X$;

[a] Also at TRIUMF, Vancouver, Canada V6T 2A3
[b] Now at Meiji Gakuin University, Yokohama 244, Japan
[c] Now at Centre de Physique des Particules de Marseille, Faculté des Sciences de Luminy, Marseille
[d] On leave from Bimingham University, Birmingham B15 2TT, UK
[e] Now at Dipartimento di Fisica, Università della Calabria and INFN, 87036 Rende, Italy
[f] And IPP, McGill University, High Energy Physics Department, 3600 University Str., Montreal, Quebec H3A 2T8, Canada
[g] Now at Department of Physics, University of Oregon, Eugene, Oregon 97405
[h] Also at Shinshu University, Matsumoto 390, Japan
[i] On leave from Research Institute for Computer Peripherals, Hangzhou, China

* In this paper, reference to a b or c quark decay implies the charge conjugate decay for $\bar{b}$ and $\bar{c}$ quarks

- photon conversions;
- Dalitz decays of π^0 and η mesons; and
- other sources such as the decay of strange hadrons.

Electrons from the first three sources are referred to as prompt electrons.

Electrons from primary b-flavoured hadron decays have a harder momentum spectrum than electrons from the other sources due to the hard b quark fragmentation. Electrons from primary b decays have a larger average momentum component perpendicular to the momentum of the decaying hadron than electrons from the other sources due to the large b-flavoured hadron mass. In this analysis, the transverse momentum p_t is measured with respect to the jet axis of the jet containing the electron candidate as explained below. We measure the production rate of electrons in the kinematic range $p > 4$ GeV/c and $p_t > 0.8$ GeV/c, where the primary decay of b-flavoured hadrons, $b \to e^- \bar{\nu}_e X$, is the dominant source of electrons. From this rate, $(\Gamma_{b\bar{b}}/\Gamma_{\text{had}}) \cdot \text{B}(b \to e^- \bar{\nu}_e X)$ can be determined, where Γ_{had} is the partial width of the Z^0 to hadrons and $\text{B}(b \to e^- \bar{\nu}_e X)$ is the average semileptonic branching fraction of the b hadrons produced on the Z^0 resonance.

Previous determinations [6–8] of $\Gamma_{b\bar{b}}$ using lepton tags at LEP are limited by the uncertainty in the semileptonic branching fraction of b hadrons, $\text{B}(b \to l \bar{\nu}_l X)$. The average semileptonic branching fraction of the mixture of B_d^0 and $B^{\pm}$ mesons produced at the $\Upsilon(4S)$ resonance has been determined [11, 12] using measured electron and muon momentum spectra. Leptons at the $\Upsilon(4S)$ with high momentum come predominantly from $b \to l \bar{\nu}_l X$. Determining the branching fraction $\text{B}(b \to l \bar{\nu}_l X)$ requires the use of a model of the semileptonic decay spectrum to extrapolate to low momenta where the presence of secondary decays $b \to c \to l \nu_l X$ and experimental limitations in lepton identification prevent a direct measurement of the rate of $b \to l \bar{\nu}_l X$ decays. For example, the models considered by the CLEO collaboration [11] result in greater than 10% variation in the value of $\text{B}(b \to l \bar{\nu}_l X)$. Our kinematic requirements, $p > 4$ GeV/c and $p_t > 0.8$ GeV/c, preferentially select electrons that have relatively high momentum in the rest frame of the decaying b hadron: precisely the region where $b \to l \bar{\nu}_l X$ dominates at the $\Upsilon(4S)$. If a particular model predicts a momentum spectrum that is too hard, this would lead to the kinematic acceptance of both CLEO and OPAL being overestimated, or alternatively, the value of $\text{B}(b \to l \bar{\nu}_l X)$ determined by CLEO and the value of $(\Gamma_{b\bar{b}}/\Gamma_{\text{had}}) \cdot \text{B}(b \to e^- \bar{\nu}_e X)$ determined by OPAL both being underestimated.

If we instead derive $\Gamma_{b\bar{b}}$ from our measurement, properly taking into account the correlation for the different models between the hardness of the lepton momentum spectrum and the values of $\text{B}(b \to l \bar{\nu}_l X)$ and $\text{B}(b \to c \to l \nu_l X)$ extracted at the $\Upsilon(4S)$, then much of the model dependence cancels in our result. In extracting $\Gamma_{b\bar{b}}$ in this way, we assume that the average semileptonic branching fraction of the b hadrons produced at $\sqrt{s} \approx M_Z$ is the same as the semileptonic branching fraction at the $\Upsilon(4S)$. This may not be true if the semileptonic branching fractions of B_s^0 and b baryons are different from those of B_d^0 and $B^{\pm}$, since B_s^0 and b baryons are presumably produced at $\sqrt{s} \approx M_Z$, but not at the $\Upsilon(4S)$. The sensitivity of $\Gamma_{b\bar{b}}$ to the above assumption is discussed.

2 The OPAL detector

The OPAL detector is described in detail in a recent publication [13]. The essential features of the components of the detector used for electron identification are described here. In the OPAL coordinate system, positive z is along the e^- beam direction, ϕ is the azimuthal angle, and θ is the polar angle.

Charged particle trajectories are measured in the central detector, which consists of three components. The innermost component is a 1 m long, high resolution drift vertex chamber with an inner radius of 8.8 cm, and outer radius of 23.5 cm, and both axial and stereo wires. This vertex chamber is surrounded by a drift (jet) chamber that is approximately 4 m long and 3.7 m in diameter and has 24 azimuthal sectors, each with 159 axial sense wires. The jet chamber covers 95% of the solid angle with at least 20 points per track and provides a measurement of the ionization energy loss of charged particles [14]. The z coordinate of each space point in the jet chamber is measured using charge division. To increase the precision of the determination of the track polar angle, the jet chamber is surrounded by drift z-chambers that provide up to six measurements of the z coordinate with 300 μm resolution per point. These z-chambers cover 94% of the solid angle in the polar angle range $|\cos\theta| < 0.72$. The central detector is contained in a pressure vessel that maintains a pressure of four atmospheres. Surrounding this pressure vessel is an aluminum coil that produces a uniform solenoidal magnetic field of 0.435 T. The resolution of the momentum in the bending plane of the magnetic field is given by $\sigma_p/p = \sqrt{(0.02)^2 + (0.0018\,p)^2}$ (p in GeV/c), and the resolution of the azimuthal angle is 0.1 mrad. When all three components of the central detector are used, the resolution of the polar angle is 0.25 mrad.

Surrounding the magnet coil is a lead-glass electromagnetic calorimeter with a presampler. The barrel lead-glass calorimeter covers the full solid angle in the region $|\cos\theta| < 0.82$. It consists of 9440 lead-glass blocks arranged in an approximate projective geometry. The energy resolution for electrons in hadronic events, σ_E, is given by $\sigma_E/E = \sqrt{(0.16)^2/E(\text{GeV}) + (0.03)^2}$. The barrel presampler is located between the magnet coil and the lead-glass calorimeter. It consists of two concentric cylinders of limited streamer tubes with wires parallel to the beam axis and cathode strips oriented at $\pm 45°$ with respect to the wires. The barrel presampler covers the full solid angle in the range $|\cos\theta| < 0.81$. Particles with $\theta = 90°$ that penetrate to the calorimeter traverse 1.7 radiation lengths of material distributed over approximately 40 cm.

Behind the electromagnetic calorimeter is the iron return yoke of the magnet, which is instrumented with streamer tubes with pads and strips to form a hadronic calorimeter. Four planes of muon chambers surround the hadronic calorimeter.

3 Data Sample

The data sample used in this analysis consists of 135 717 events passing a hadronic event selection [1]. These data were collected during the 1990 run of LEP at centre-of-mass energies ranging from 88.2 GeV to 94.2 GeV. The hadronic event selection is 98.4% efficient and contains approximately 0.2% background, which is from leptonic Z^0 decays and two-photon scattering events. This sample corresponds to 137 600 produced hadronic events with an error of 0.4%. To significantly reduce the chance that electrons from $Z^0 \to \tau^+\tau^-$, $\tau \to e\nu\bar{\nu}$ contaminate the electron sample, events are required to have at least six good charged tracks in addition to passing the hadronic event selection criteria. A good track satisfies the following requirements: the distance of closest approach of the track to the beamspot in the plane perpendicular to the beam axis must be less than 5 cm; at this point the z coordinate of the track must be less than 50 cm from the nominal collision point; the track must have at least 40 space points measured in the jet chamber and a transverse momentum with respect to the beam axis greater than 0.15 GeV/c. The track multiplicity requirement reduces the sample examined for electron candidates to 133 313 events.

Jets are found using the scaled-mass jet finding algorithm of JADE [15], with the E0 recombination scheme [16], using only good charged tracks and a value of $y_{\text{cut}} = 0.02$. With this value of y_{cut}, the axis of a jet containing an electron is an approximate representation of the line-of-flight of the parent hadron. For each good track, we define p_t as the component of its momentum transverse to the direction of the jet containing the track. In this definition, the track is included in the determination of the jet axis.

4 Electron selection

The electron selection is based on the ionization loss ($\mathrm{d}E/\mathrm{d}x$) measured in the jet chamber, the amplitude of the barrel presampler cluster associated to the central detector track, the lateral distribution of energy in the barrel lead-glass cluster associated to the track, and the comparison of the track momentum with the lead-glass cluster energy. At smaller momenta, the $\mathrm{d}E/\mathrm{d}x$ measurement alone would be sufficient to produce a sample of electrons with low background from misidentified hadrons. At larger momenta, the presampler and lead-glass calorimeter selection criteria are necessary to keep this hadronic background low.

Tracks considered as electron candidates must satisfy the track requirements given in Sect. 3. Since all the electron selection criteria require an accurate estimate of the polar angle, tracks considered as electron candidates are required to have at least three associated z-chamber (CZ) hits: $N_{\text{CZ}} \geqq 3$. The z-chambers cover the polar angle range $|\cos\theta| < 0.72$, but tracks are required to satisfy $|\cos\theta| < 0.7$ to avoid the edge of the z-chamber acceptance.

For charged tracks, the ionization energy loss, $\mathrm{d}E/\mathrm{d}x$, is measured in the jet chamber with up to 159 samples per track. A truncated mean (the mean of the lower 70% of the samples) is used to estimate the $\mathrm{d}E/\mathrm{d}x$ of each track.

The $\mathrm{d}E/\mathrm{d}x$ selection is based on

$$N^{\sigma}_{\mathrm{d}E/\mathrm{d}x} = \frac{\mathrm{d}E/\mathrm{d}x\ (\text{measured}) - \langle \mathrm{d}E/\mathrm{d}x \rangle_e}{\sigma_{\mathrm{d}E/\mathrm{d}x}}; \tag{1}$$

where $\langle \mathrm{d}E/\mathrm{d}x \rangle_e$ is the mean $\mathrm{d}E/\mathrm{d}x$ expected for electrons, and the error in $\mathrm{d}E/\mathrm{d}x$ is approximated by [14]:

$$\frac{\sigma_{\mathrm{d}E/\mathrm{d}x}}{\mathrm{d}E/\mathrm{d}x} = 0.038 \cdot (159/N_{\text{samp}})^{0.43}, \tag{2}$$

with N_{samp} being the number of samples used to measure $\mathrm{d}E/\mathrm{d}x$. Tracks considered as electron candidates must have a minimum of 40 samples, $N_{\text{samp}} \geqq 40$. Figure 1 shows $N^{\sigma}_{\mathrm{d}E/\mathrm{d}x}$ for tracks in hadronic events after some of the other electron selection criteria have been applied to enhance the signal. Pion and electron peaks and a shoulder due to kaons are clearly visible. Electron candidates are required to have

- $N^{\sigma}_{\mathrm{d}E/\mathrm{d}x} > -2.0$.

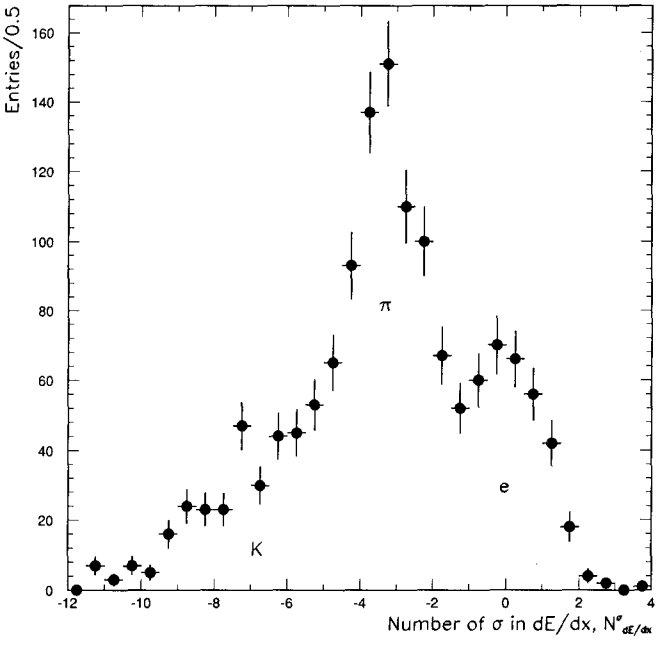

Fig. 1. $N^{\sigma}_{\mathrm{d}E/\mathrm{d}x}$ for tracks with $p > 4$ GeV/c and $p_t > 0.8$ GeV/c in hadronic events after other electron selection criteria (all requirements except the E_{cone}/p cut) have been applied to enhance the signal

That is, the track is rejected as an electron candidate if the dE/dx value is more than 2.0 standard deviations below the value expected for electrons.

The barrel presampler is sensitive to whether a particle has begun to shower before entering the lead-glass calorimeter. The presampler is calibrated so that the distribution of the amplitudes of clusters created by beam-energy muons peaks at two units of amplitude, corresponding to the two concentric cylindrical layers of limited-streamer tubes composing the presampler. Hadrons usually do not interact in the central detector pressure vessel and the magnet coil, which are located inside the presampler, and therefore leave a signal similar to muons in the presampler; electrons usually interact in this material and leave a presampler signal of much larger amplitude. The average amplitude for electrons increases with increasing electron momentum. The electron candidate track is required to be associated to a presampler cluster with

- presampler cluster amplitude greater than $2.5 + p/2$ or 10, whichever is smaller,

where p is the momentum in GeV/c. The effect of the requirement is illustrated in Fig. 2, which shows the presampler amplitude distribution after all other electron selection criteria have been applied (the calorimeter selection is described below). The required amplitude increases with momentum in order to reject as much background as possible, while allowing an efficiency that does not depend on momentum.

The inner edges of the barrel lead-glass blocks lie on a cylinder of radius 246 cm. The blocks are 24.7 radiation lengths (X_0) deep and 6.7 X_0 wide. The face of each block is 10 cm by 10 cm, so a block subtends 41 mrad in θ at $\cos\theta = 0$ and 29 mrad at $\cos\theta = 0.7$. With this combination of angular granularity and block width in X_0, most of the energy of an electron shower is contained, on average, in a smaller number of blocks than the energy of a showering hadronic particle or the combined energy of a charged hadronic particle with nearby electromagnetic showers from π^0's. This difference in the lateral distribution of the energy in the lead-glass is used to separate electrons from hadronic background.

The lateral distribution of the energy in the lead-glass cluster associated to a track is measured by comparing two energies, E_{cone} and $E_{\text{cone}2}$. E_{cone} is the sum of the detected energies in all blocks in the associated lead-glass cluster that have centres within 30 mrad of the extrapolated track position at the inner face of the lead-glass. The second energy, $E_{\text{cone}2}$, is equal to E_{cone} plus the sum

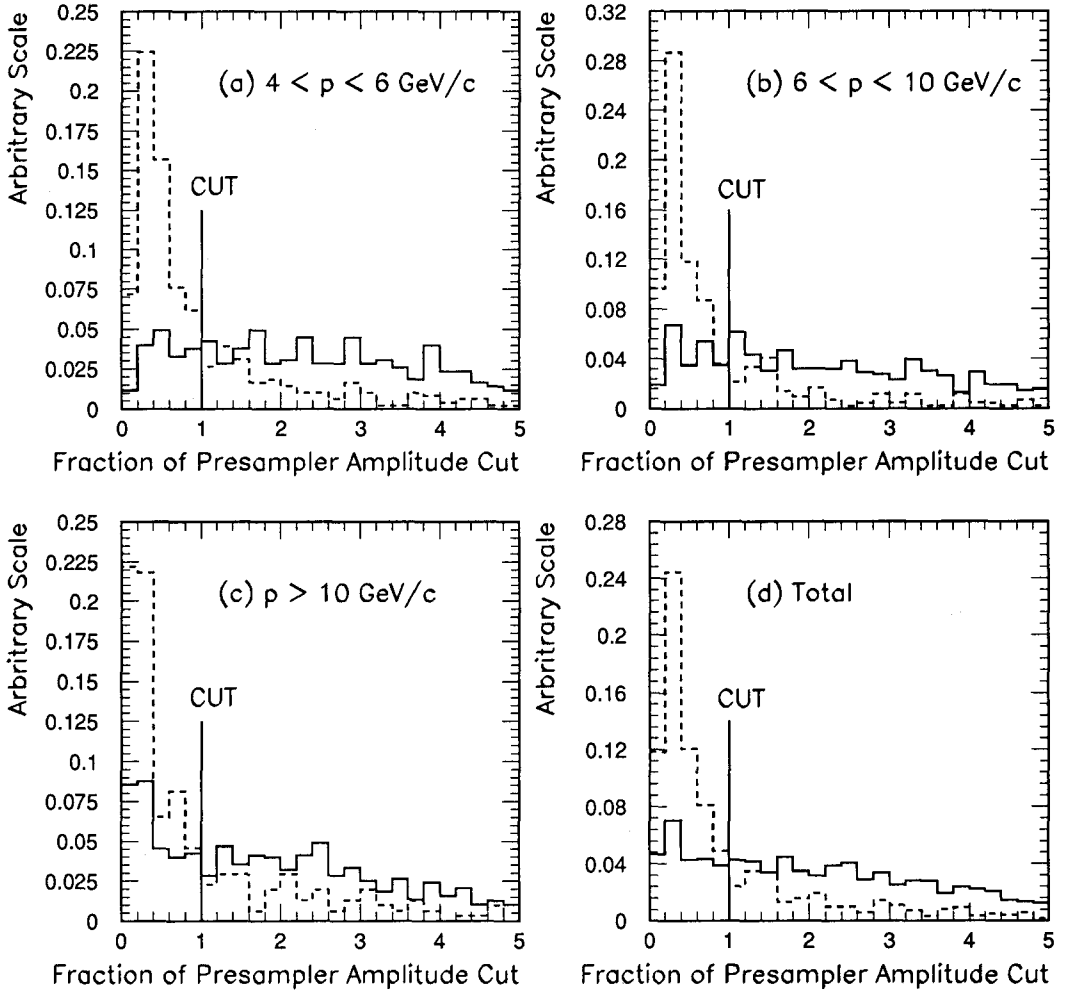

Fig. 2a–d. Effect of the presampler requirement for tracks with $p_t > 0.8$ GeV/c. The three plots **a** to **c** correspond to the three momentum bins, and plot **d** is for $p > 4$ GeV/c. The horizontal axis is the presampler amplitude associated to the track divided by the presampler requirement value (the smaller of $2.5 + p/2$ or 10). Tracks passing the presampler requirement are above 1 on the horizontal axis. The solid histogram is for tracks passing all the electron selection criteria but the presampler criteria. The dashed histogram is for tracks with $N^{\sigma}_{dE/dx} < -2.5$, but passing the lead-glass calorimeter selection

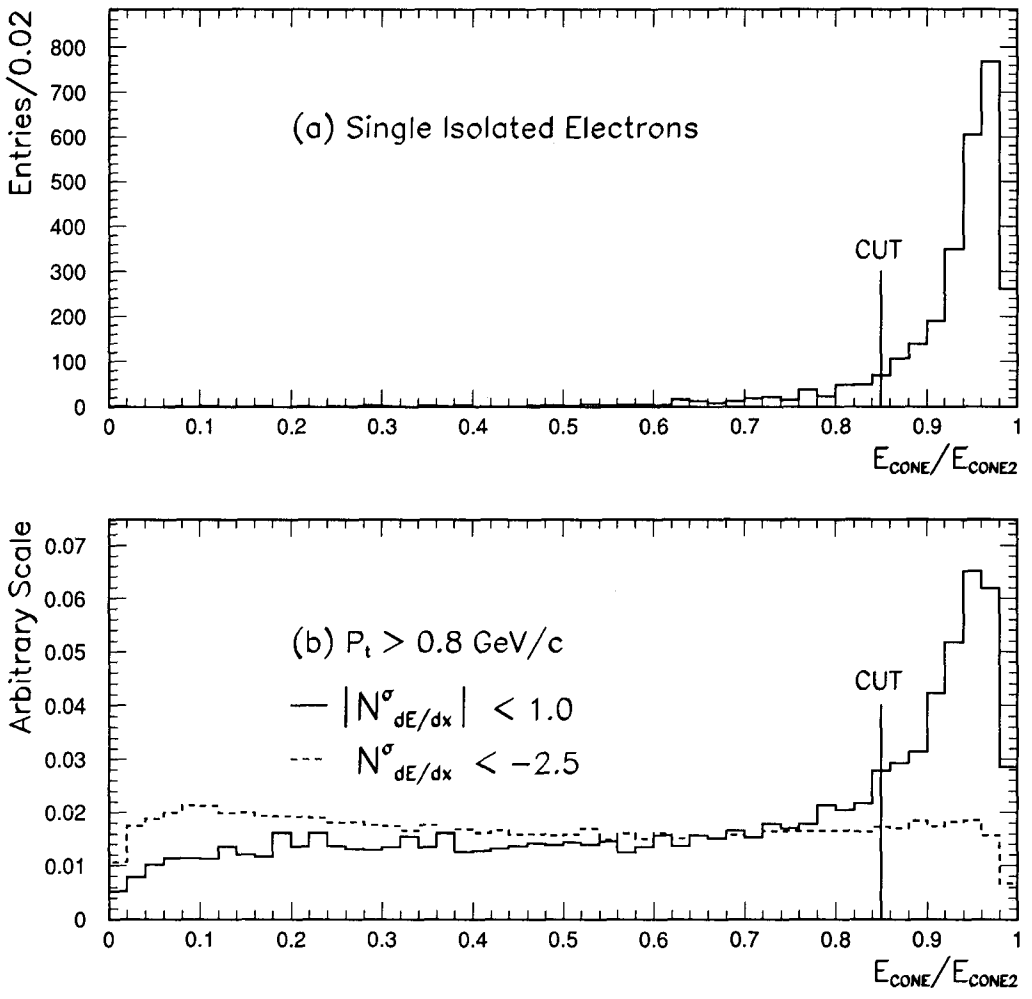

Fig. 3. a $E_{\text{cone}}/E_{\text{cone}\,2}$ for tracks from single electron events. **b** $E_{\text{cone}}/E_{\text{cone}\,2}$ for tracks ($p_t > 0.8$ GeV/c) with $\mathrm{d}E/\mathrm{d}x$ more than 2.5 standard deviations below the expected value for electrons (dashed line) and for tracks with $\mathrm{d}E/\mathrm{d}x$ within 1.0 standard deviation of the expected value (solid line). The presampler amplitude requirement has already been applied. In both figures, the cut at 0.85 is indicated

of the detected energies in all blocks that touch (either on the side or on the corner) any block that was used in E_{cone}. These energies are corrected for the average undetected energy of an electron shower due to the material in front of the calorimeter. On average, a large percentage of the energy of an electron is contained in E_{cone}, so unless there are other particles surrounding the electron that contribute a significant amount of energy to the blocks defining $E_{\text{cone}\,2}$, the ratio $E_{\text{cone}}/E_{\text{cone}\,2}$ is close to unity for electrons. This is illustrated in Fig. 3a, which shows the $E_{\text{cone}}/E_{\text{cone}\,2}$ distribution for events with a single, isolated electron in the barrel region of the detector. These single electrons are from radiative Bhabha scattering, $e^+e^- \to e^+e^-\gamma$, and the two-photon process, $e^+e^- \to e^+e^-e^+e^-$. The selection of these events is very similar to the selection described in [17]. Figure 3b shows $E_{\text{cone}}/E_{\text{cone}\,2}$ for tracks with $\mathrm{d}E/\mathrm{d}x$ more than 2.5 standard deviations below the expected value for electrons compared with tracks with $\mathrm{d}E/\mathrm{d}x$ within 1.0 standard deviation of the expected value for electrons. The hadronic background has a flat distribution in $E_{\text{cone}}/E_{\text{cone}\,2}$, while the electrons peak towards one. The value of $E_{\text{cone}}/E_{\text{cone}\,2}$ is found to be relatively independent of p. Electron candidates are required to satisfy

- $(E_{\text{cone}}/E_{\text{cone}\,2}) > 0.85$.

The final electron selection requirement is based on E_{cone}/p. For an electron, the energy E measured in the lead-glass calorimeter should equal the momentum, within the detector resolution (except for electrons that have lost energy via bresmstrahlung, in which case $E > p$). For hadrons, E is usually much less than p, unless the hadron showers in the lead-glass or is nearby other electromagnetically interacting particles. Using E_{cone} instead of the cluster energy reduces this overlap background and avoids mismeasuring the electron if there are other nearby particles. Figure 4a shows the distribution of E_{cone}/p from the single electron events, and Fig. 4b shows the distribution of E_{cone}/p for tracks with $\mathrm{d}E/\mathrm{d}x$ more than 2.5 standard deviations below that expected for an electron. Since E_{cone} is usually slightly less than the energy of the electron, the distribution of E_{cone}/p has a peak slightly below unity. An electron candidate is required to have

- $0.7 < E_{\text{cone}}/p < 1.4$.

5 Signal and background determination

The total number of tracks with $p_t > 0.8$ GeV/c passing the electron selection criteria is 1411. Table 1 gives the number of electron candidates in three bins in momentum.

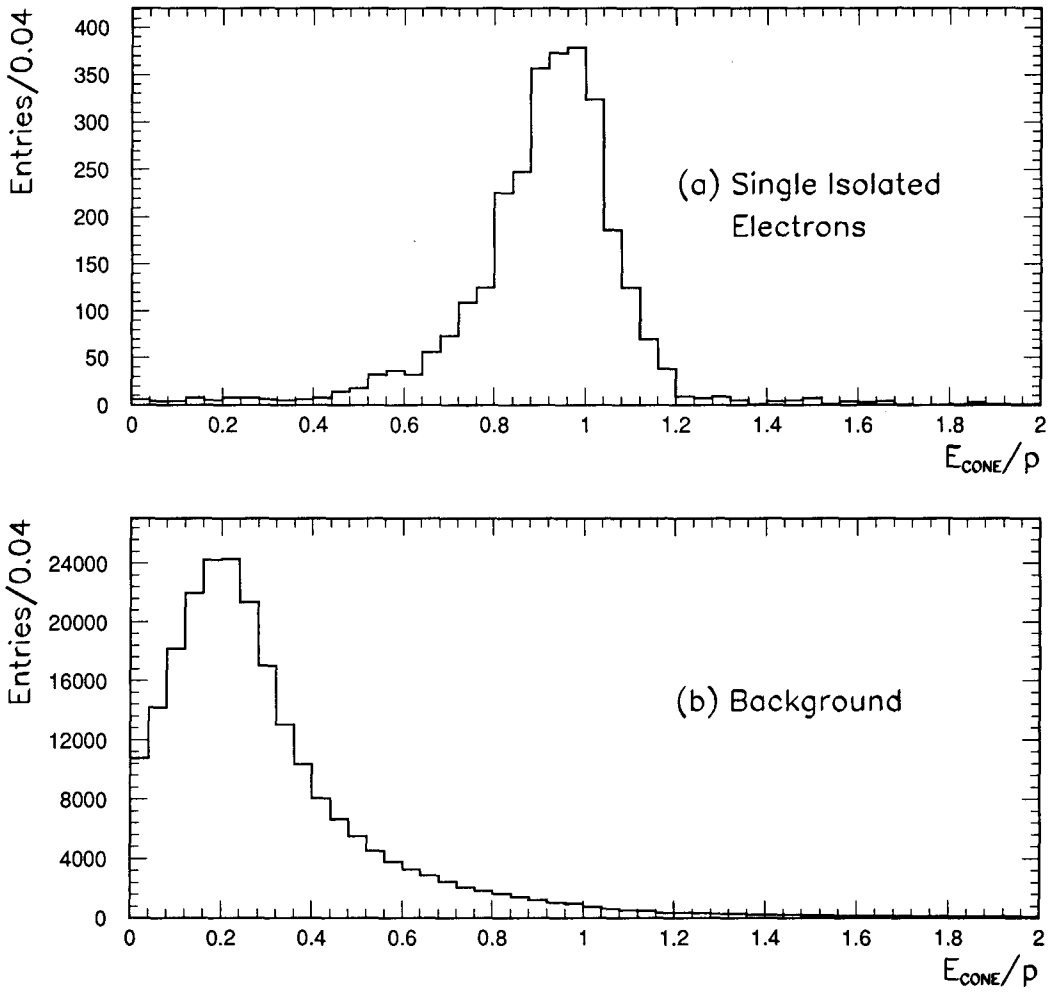

Fig. 4. **a** E_{cone}/p for tracks from single electron events. **b** E_{cone}/p for tracks ($p_t > 0.8$ GeV/c) with dE/dx more than 2.5 standard deviations below the expected value for electrons to illustrate the shape of the background component in the E_{cone}/p distribution

Table 1. The number of electron candidates with $p_t > 0.8$ GeV/c in three bins of momentum. The second row is the background from photon conversions. The first error is the statistical error and the second error is the systematic error. The third and fourth rows are two independent estimates of hadronic background from the data. The error is the statistical error. The last row is the electron signal after the backgrounds from photon conversions and misidentified hadrons determined using the E_{cone}/p fit have been subtracted. The error is the statistical error only

Momentum (GeV/c)	$4 < p < 6$	$6 < p < 10$	$p > 10$
tracks passing selection	324	508	579
conversion background	$60.0 \pm 5.5 \pm 15.0$	$30.0 \pm 3.9 \pm 7.5$	$24.0 \pm 3.5 \pm 6.0$
hadronic background			
• from $N^{\sigma}_{dE/dx}$	13.4 ± 1.6	28.4 ± 3.6	67.0 ± 8.3
• from E_{cone}/p	9.7 ± 1.8	30.5 ± 5.1	77.2 ± 7.0
electron signal	254 ± 17	448 ± 22	478 ± 24

Of these 1411 tracks, 57 are identified as originating from photon conversions and are rejected. Photon conversions are identified using information from the central detector only. The identification demands a pair of oppositely charged tracks with a momentum sum vector that points back to the event vertex. To reduce combinatorial background, conversion candidate pairs must have a reconstructed radius of origin greater than 1 cm from the nominal beamspot, and both tracks must have dE/dx consistent with the value expected for an electron. The most important identification criterion is that the invariant mass of the pair, assuming it is an electron-positron pair, be less than 50 MeV/c^2.

The photon conversion identification efficiency is determined using a sample of simulated hadronic events. These events were generated using the JETSET Monte Carlo program [18] and a program that simulates [19] the response of the OPAL detector. The identification efficiency determined with this Monte Carlo data sample is about 50%, so the remaining background from photon conversions is equal to the number of observed identified conversions. The correction for unidentified conversions also includes electrons from the Dalitz decays of neutral mesons; this background is less than 1% of the total number of electrons. Table 1 lists the background from photon conversions in three bins of momentum. The first error on this background is the statistical error from the number of observed conversion candidates. The second error is a 25% systematic error assigned because of uncertainties in the Monte Carlo modelling of the central detector and uncertainties in the conversion identification

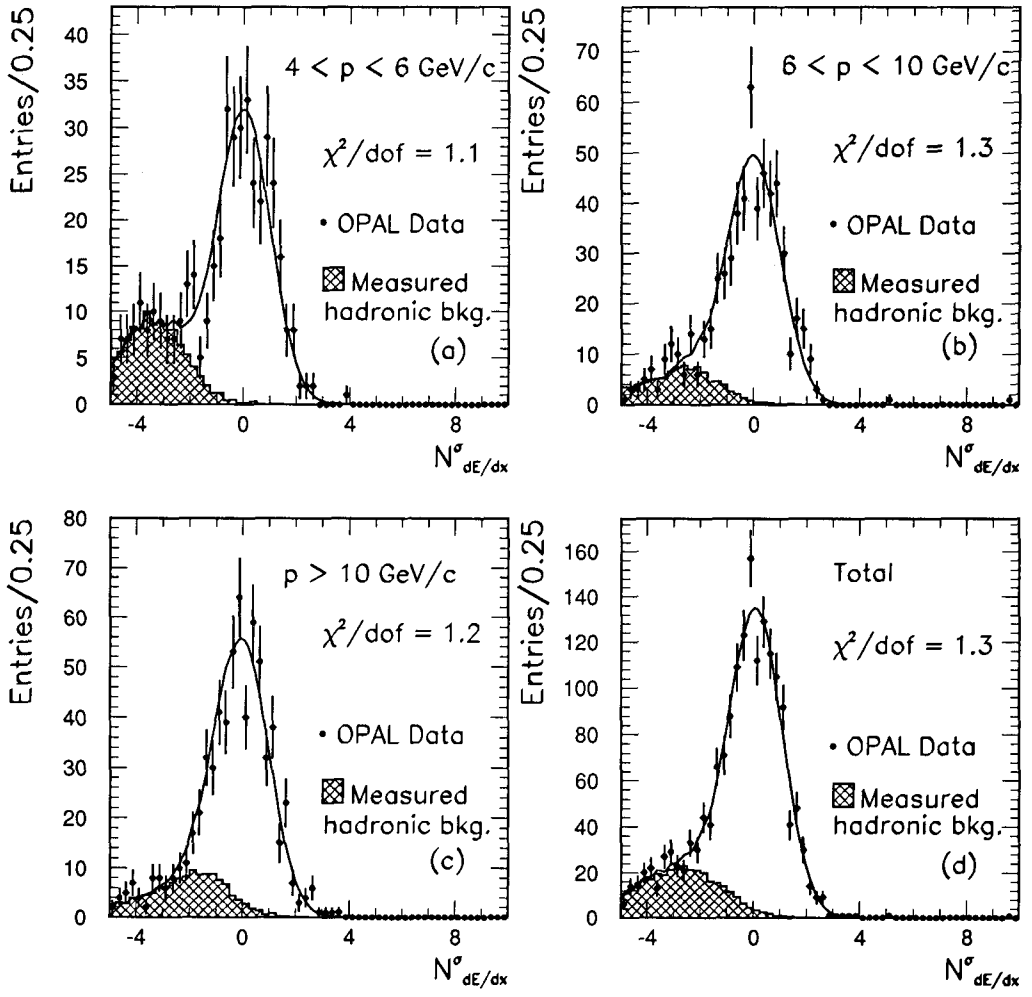

Fig. 5a–d. The fits to the $N^{\sigma}_{\mathrm{d}E/\mathrm{d}x}$ distributions in three momentum bins. Plot **d** is the sum of the other three plots. The points are electron candidates passing all electron selection criteria but the $N^{\sigma}_{\mathrm{d}E/\mathrm{d}x}$ requirement. The hatched histograms show the background component, determined from the data, as described in the text

efficiency. The fraction of prompt electrons rejected as photon conversions has been determined to be less than 0.5% and is neglected.

After subtraction of the background due to photon conversions, the remaining sample of tracks still has background from hadrons misidentified as electrons. This misidentification background is determined from the data by exploiting the independence of the $\mathrm{d}E/\mathrm{d}x$ and calorimeter selection criteria. The amount of signal and hadronic background in the electron sample is measured using two independent methods: the first uses $N^{\sigma}_{\mathrm{d}E/\mathrm{d}x}$ distributions and the second uses E_{cone}/p distributions. In the first method, the hadronic background as a function of p and p_t is estimated by fits to $N^{\sigma}_{\mathrm{d}E/\mathrm{d}x}$ distributions after applying all requirements except the $N^{\sigma}_{\mathrm{d}E/\mathrm{d}x}$ requirement. The shape of the background component in p and p_t bins is determined from the data using tracks that are anti-selected by requiring that the track fail the presampler requirement and have $0.1 < E_{\mathrm{cone}}/p < 0.5$ (but the track must still fulfil the $E_{\mathrm{cone}}/E_{\mathrm{cone}\,2} > 0.85$ requirement). The distribution of $N^{\sigma}_{\mathrm{d}E/\mathrm{d}x}$ for electrons should be a Gaussian with a mean of zero and unit width. This is found to be true using electrons from identified photon conversions. This Gaussian and the hadronic background shape histograms are fitted to the $N^{\sigma}_{\mathrm{d}E/\mathrm{d}x}$ distributions; only the normalizations of the Gaussian and background histograms are allowed to vary. The fits in the three momentum bins for $p_t > 0.8$ GeV/c are shown in Fig. 5, and the resulting measurement of the hadronic background in three momentum bins is given in Table 1. The errors on these background numbers in the table are dominated by the statistical errors from the fits: systematic shifts in these numbers due to varying the anti-selection requirements and due to including the mean and width of the Gaussian as free parameters in the fit are negligible.

A second, independent, background determination is made by fitting to the E_{cone}/p distributions after all selection criteria are applied except the E_{cone}/p requirement. The shape of the background component is determined from tracks anti-selected by requiring that they satisfy $N^{\sigma}_{\mathrm{d}E/\mathrm{d}x} < -2.5$. Only the background normalization is allowed to vary in the fit. The signal is fit to a function of six parameters that adequately describes the changing shape of the electron peak in the E_{cone}/p distributions in the different momentum bins. The resulting background is depicted in Fig. 6 and is given in Table 1. The background fractions from the two methods agree within the statistical errors. The hadronic background measured with the fits to the E_{cone}/p distributions is used in the subtraction to determine the signal, and the in-

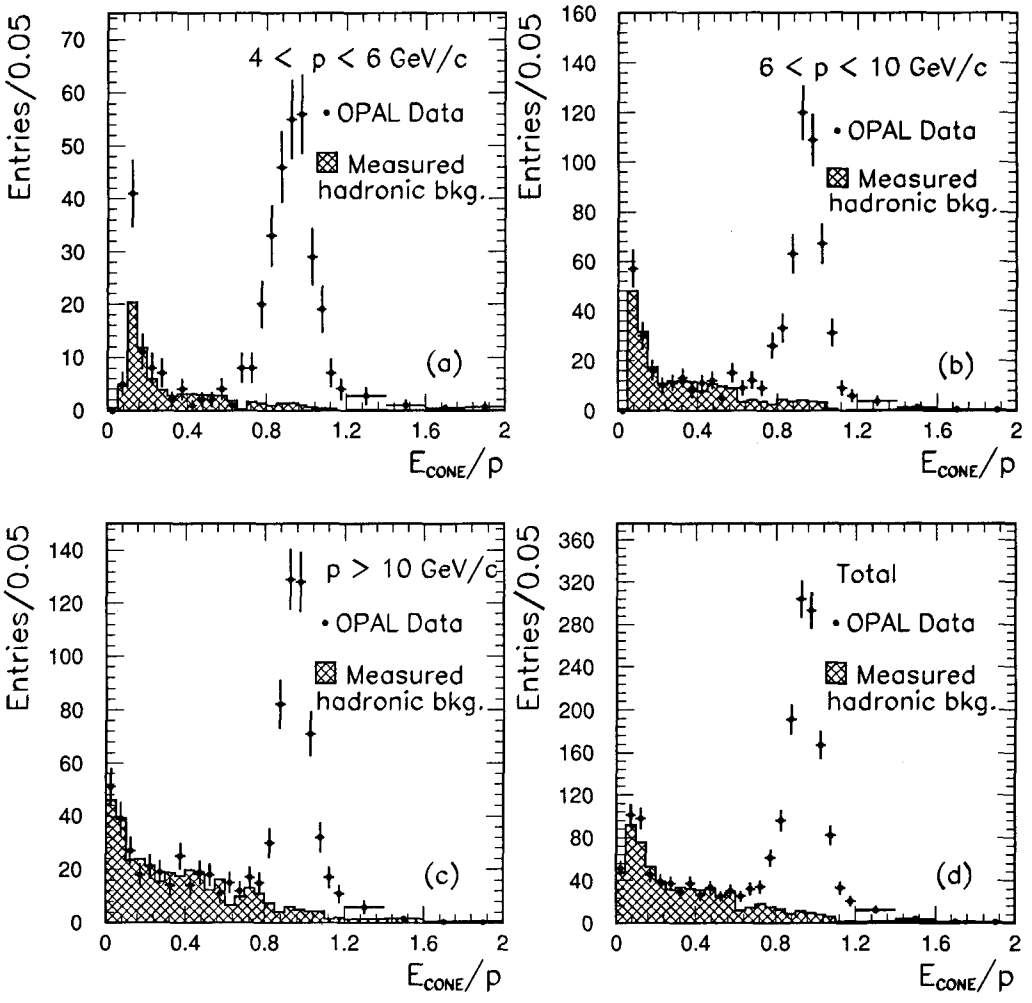

Fig. 6a–d. The determination of the hadronic background using the E_{cone}/p distributions in three momentum bins. Plot **d** is the sum of the other three plots. The points are electron candidates passing all electron selection criteria but the E_{cone}/p requirement. The hatched histograms show the background component, determined from the data, as described in the text

dependent measurement using $N^{\sigma}_{\mathrm{d}E/\mathrm{d}x}$ fits is used to assess systematic errors. The hadronic background fraction for electrons with $p > 4$ GeV/c and $p_t > 0.8$ GeV/c is 9%.

The last line in Table 1 lists the electron signal after the backgrounds from photon conversions and misidentified hadrons determined using the E_{cone}/p fits have been subtracted. The error is the statistical uncertainty only. The systematic error assigned to the signal due to uncertainty in the hadronic background is 1.1%.

6 Number of produced prompt electrons

Table 1 lists the numbers of electron candidates after the backgrounds from photon conversions and misidentified hadrons have been subtracted. Using Monte Carlo simulated hadronic events, the number of electrons expected from other sources such as the decay of strange hadrons is found to be negligible after the momentum and transverse momentum requirements. The numbers of Table 1 must be corrected for the efficiency of the electron identification criteria to obtain the total number of prompt electrons produced, N^{e}_{prompt}, with $p > 4$ GeV/c, $p_t > 0.8$ GeV/c, and $|\cos\theta| < 0.7$.

6.1 Electron identification efficiency

The efficiencies of the different selection criteria are determined from the data, separately in each of the three momentum bins, and are summarized in Table 2.

The combined efficiency of the $N_{\text{samp}} \geqq 40$ and $N_{\text{CZ}} \geqq 3$ selection criteria is determined by finding the efficiency of these requirements on tracks passing the muon selec-

Table 2. Electron identification efficiencies for $p_t > 0.8$ GeV/c as a function of p for tracks with $|\cos\theta| < 0.7$. The errors are the statistical errors only. The efficiencies for the four requirements are multiplied together to give the combined efficiency. The units for p are GeV/c

	$4 < p < 6$	$6 < p < 10$	$p > 10$
N_{CZ} and N_{samp}	0.76 ± 0.03	0.81 ± 0.02	0.79 ± 0.02
$N^{\sigma}_{\mathrm{d}E/\mathrm{d}x}$	0.969 ± 0.007	0.969 ± 0.007	0.969 ± 0.007
$E_{\text{cone}}/E_{\text{cone 2}}$ and E_{cone}/p presampler	0.761 ± 0.022	0.827 ± 0.028	0.836 ± 0.023
combined efficiency	0.838 ± 0.027	0.846 ± 0.026	0.828 ± 0.028
	0.470 ± 0.028	0.549 ± 0.029	0.530 ± 0.027

tion described in [8]. The efficiency of a track to satisfy the N_{samp} and N_{CZ} criteria is sensitive to the activity in the central detector around this track. Monte Carlo studies show that this level of activity is different for $b \to e\nu_e X$ than it is for other processes like $b \to c \to e\nu_e X$ or $c \to e\nu_e X$, even for tracks with the same momentum and transverse momentum. The muons are an ideal sample to use to calculate this efficiency, since the underlying physics processes resulting in muons in hadronic events should be similar to those processes producing electrons (excluding electrons from photon conversions and muons from nonprompt decays).

The distribution of $N^{\sigma}_{\mathrm{d}E/\mathrm{d}x}$ for electrons is very close to a unit Gaussian. To evaluate the non-Gaussian tails of the $N^{\sigma}_{\mathrm{d}E/\mathrm{d}x}$ distribution, we have studied samples of electrons identified from photon conversions, and pions from identified [20] $K^0 \to \pi^+\pi^-$ decays. Using a pure sample of electrons from photon conversions identified in the jet chamber gas volume without using $\mathrm{d}E/\mathrm{d}x$ as a selection criterion, the efficiency of the requirement is found to be 0.963 ± 0.015. A statistically more precise determination of the efficiency of the $N^{\sigma}_{\mathrm{d}E/\mathrm{d}x}$ requirement is made using pions from $K^0 \to \pi^+\pi^-$ decays using the expected value of $\langle \mathrm{d}E/\mathrm{d}x \rangle$ for pions rather than the expected value for electrons in the formation of $N^{\sigma}_{\mathrm{d}E/\mathrm{d}x}$. For $p > 4\,\mathrm{GeV/c}$, only particles with larger mass than the mass of the pion will contaminate the low end of the $N^{\sigma}_{\mathrm{d}E/\mathrm{d}x}$ distributions for pions. Any $K^0 \to \pi^+\pi^-$ candidate that also satisfies the $\Lambda \to p\pi$ hypothesis is not considered. The remaining small amount of combinatorial background in the $K^0 \to \pi^+\pi^-$ sample is almost entirely due to pions. The efficiency of the requirement is found to be 0.969 ± 0.007, with no significant variation with momentum. This efficiency is in good agreement with the value of 0.977 expected for a cut at -2 standard deviations on a unit Gaussian. The possible systematic bias of the $N^{\sigma}_{\mathrm{d}E/\mathrm{d}x}$ distribution not being centred at zero is considered in the following subsection.

The muons in hadronic events are also used in the calculation of the combined efficiency of the $E_{\text{cone}}/E_{\text{cone}2}$ and E_{cone}/p requirements. Electrons fail these requirements either because the lateral spread of the electron shower is unusually wide, or because energy deposits of nearby particles increase $E_{\text{cone}2}$. These overlap effects are measured from the data by studying the energy deposits in E_{cone} and $E_{\text{cone}2}$ using the muon sample. The loss of efficiency due to lateral shower spread is determined using single electron events. The possibility that the combination of overlapping energy and lateral shower spread cause an electron to fail the $E_{\text{cone}}/E_{\text{cone}2}$ requirement has been taken into account. The efficiency determined in this way has been corrected for the effect of the nonprompt background in the muon sample. This background is less isolated than prompt muons and therefore causes an underestimate of the $E_{\text{cone}}/E_{\text{cone}2}$ efficiency. The correction is based on fully simulated JETSET Monte Carlo events and ranges from 3% in the lowest momentum bin to 2% in the highest momentum bin.

The efficiency of the presampler requirement is found by determining the amount of signal between $0.7 < E_{\text{cone}}/p < 1.4$ in the E_{cone}/p distribution after all selection criteria (N_{CZ}, N_{samp}, $N^{\sigma}_{\mathrm{d}E/\mathrm{d}x}$, and $E_{\text{cone}}/E_{\text{cone}2}$) but the presampler requirement have been applied, and then comparing this signal to the number of electrons found in the E_{cone}/p distribution of tracks rejected by the presampler requirement. The fits to these two E_{cone}/p distributions are shown in Fig. 7a, b for $p > 10$ and $p_t > 0.8\,\mathrm{GeV/c}$. The shapes of the background distributions are determined with tracks that have $N^{\sigma}_{\mathrm{d}E/\mathrm{d}x} < -2.5$, and the same fit procedure described earlier to determine hadronic background is used. The presampler efficiencies determined with these fits agree within statistics with the presampler efficiencies determined from a sample of electrons from identified photon conversions.

The efficiencies of the (1) N_{CZ} and N_{samp} requirements, (2) the $N^{\sigma}_{\mathrm{d}E/\mathrm{d}x}$ requirement, (3) the $E_{\text{cone}}/E_{\text{cone}2}$ and E_{cone}/p requirements, and (4) the presampler requirement are multiplied together to obtain the total electron identification efficiency. The possible correlations between the requirements are taken into account in the procedure for calculating the efficiencies; for example, the efficiency for the presampler requirement is calculated for tracks that have already passed requirements (1) to (3). These correlations were checked with the Monte Carlo, as well, and were found to be small. Table 2 gives the efficiencies of requirements (1) to (4) and the total efficiency in the three momentum bins. The errors are the statistical errors only. The efficiency of requirements (1) and (2) show no dependence on p_t in the region above $p_t > 0.8\,\mathrm{GeV/c}$. The efficiency of the $E_{\text{cone}}/E_{\text{cone}2}$ and E_{cone}/p requirements and the presampler requirement have a slight dependence on p_t for $p_t > 0.8$ as shown in Table 3. The average efficiencies given in Table 2 for these two requirements take into account the observed number of electrons in each p and p_t bin. The efficiency for finding an electron with $p > 4\,\mathrm{GeV/c}$, $p_t > 0.8\,\mathrm{GeV/c}$, and $|\cos\theta| < 0.7$ is 0.522 ± 0.016 (statistical uncertainty only).

Table 3. The efficiency of the combined $E_{\text{cone}}/E_{\text{cone}2}$ and E_{cone}/p requirements and the presampler requirement as a function of p and p_t in the range $|\cos\theta| < 0.7$. The average efficiencies take into account the observed number of events in each p_t bin. The errors are the statistical errors only. The units for p and p_t are GeV/c

Efficiency of the combined $E_{\text{cone}}/E_{\text{cone}2}$ and E_{cone}/p requirements

	$4 < p < 6$	$6 < p < 10$	$p > 10$
$0.8 < p_t < 1.2$	0.748 ± 0.029	0.815 ± 0.039	0.835 ± 0.028
$1.2 < p_t < 1.6$	0.772 ± 0.038	0.825 ± 0.057	0.835 ± 0.048
$p_t > 1.6$	0.808 ± 0.038	0.864 ± 0.049	0.838 ± 0.050
Average over p_t	0.761 ± 0.022	0.827 ± 0.028	0.836 ± 0.023

Efficiency of the presampler requirement

	$4 < p < 6$	$6 < p < 10$	$p > 10$
$0.8 < p_t < 1.2$	0.824 ± 0.033	0.847 ± 0.042	0.788 ± 0.026
$p_t > 1.2$	0.863 ± 0.049	0.846 ± 0.031	0.865 ± 0.050
Average over p_t	0.838 ± 0.027	0.846 ± 0.026	0.828 ± 0.028

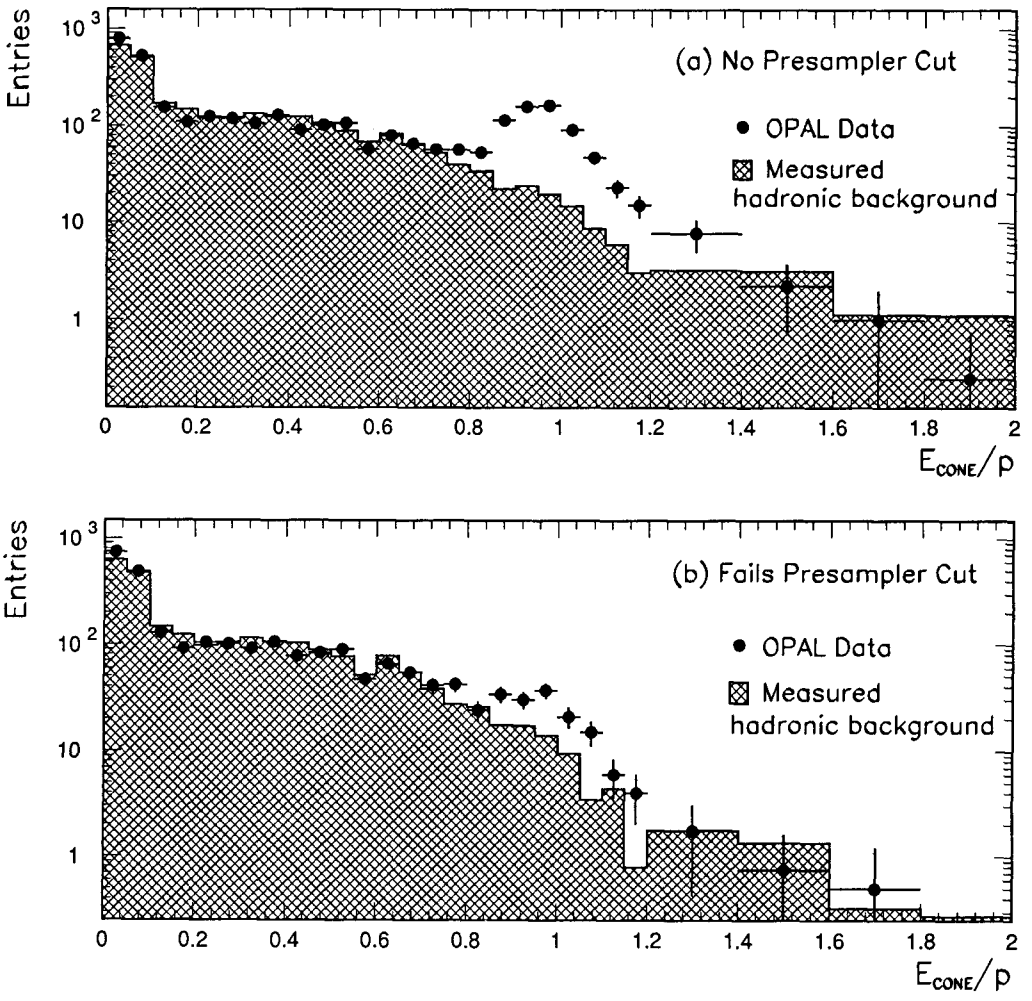

Fig. 7. a The E_{cone}/p distribution (points) for tracks with $p > 10$ GeV/c and $p_t > 0.8$ GeV/c after all requirements but the presampler requirement and the E_{cone}/p requirement have been applied. The hatched histogram is the distribution of E_{cone}/p for tracks that have $N^{\sigma}_{dE/dx} < -2.5$. **b** The tracks in **a** that fail the presampler requirement. The excess of the points above the background histogram gives the inefficiency of the presampler requirement

6.2 Systematic errors on the efficiency

Three sources of possible systematic bias in the electron identification efficiency are considered. A systematic error in the dE/dx efficiency for an electron could be caused by the uncertainties in the expected $\langle dE/dx \rangle$ and dE/dx resolution for electrons in hadronic events. This error has been estimated by allowing the mean, the width, and the normalization to vary in the fits to the $N^{\sigma}_{dE/dx}$ distribution described earlier and shown in Fig. 5. The maximum change in efficiency is 1.1%. Assuming any systematic effect is correlated from momentum bin to momentum bin, a 1.1% systematic error is added to the efficiency-corrected number of electrons, given below.

In determining the presampler efficiency, it has been assumed that the E_{cone}/p distribution of the background selected with the $N^{\sigma}_{dE/dx} < -2.5$ antiselection matches the shape of the E_{cone}/p distribution of the true background. This assumption could introduce a bias in the determination of the efficiency for momenta greater than 10 GeV/c where the antiselected sample consists mainly of charged kaons and protons, but the background to the electron signal consists mainly of pions. Kaons and protons are expected to have softer E_{cone}/p distributions than pions, and using these softer distributions could result in a systematic underestimate of the presampler efficiency. An upper limit on the presampler efficiency for electrons in hadronic events is the presampler efficiency for electrons in single electron events. In the $p > 10$ GeV/c bin, the difference of the presampler efficiency determined from the fit and the presampler efficiency from the single electron events is 5% and has been taken as the maximum possible effect of the above systematic bias. Using this maximum difference, a systematic error of 1.8% is added to the efficiency-corrected number of electrons. For momenta below 10 GeV/c, the dE/dx resolution makes it possible to produce a background sample consisting mostly of kaons and protons and a background sample consisting mainly of pions. No systematic difference between the efficiencies determined with these two different background distributions is observed.

The correction to the combined E_{cone}/E_{cone2} and E_{cone}/p requirements due to the background in the prompt muon sample is based on a Monte Carlo estimate of the background. This estimate has a 25% uncertainty for $p > 4$ GeV/c, which leads to a 1.0% error in the efficiency-corrected number of electrons.

The above systematic errors are all smaller than the statistical errors on the efficiencies given in Table 2.

6.3 Corrected number of prompt electrons

The total number of prompt electrons produced with $p > 4\,\mathrm{GeV/c}$, $p_t > 0.8\,\mathrm{GeV/c}$, and $|\cos\theta| < 0.7$ after correcting for the electron identification efficiency is

- $N^e_{\mathrm{prompt}} = 2258 \pm 71 \pm 90 \pm 59$.

The first error is statistical, the second is due to the uncertainty in the electron identification efficiency, and the third is due to the uncertainty in the number of electrons originating from photon conversions.

The 4.0% error on N^e_{prompt} due to the uncertainty of the electron identification efficiency is a sum in quadrature of the three systematic errors with the 3.1% error due to the statistical uncertainty on the efficiency.

7 Measurement of $\Gamma_{b\bar{b}}/\Gamma_{\mathrm{had}}$

The number of prompt electrons, N^e_{prompt}, is the sum of three sources: (1) electrons from semileptonic decays of b hadrons, (2) electrons from the decays of charmed hadrons and from τ leptons, both coming from b hadrons, and (3) the semileptonic decays of charmed hadrons containing charm quarks produced directly from the Z^0. This sum can be expressed as follows:

$$\begin{aligned} N^e_{\mathrm{prompt}} = {} & 2 \cdot N_{\mathrm{had}} \cdot \frac{\Gamma_{b\bar{b}}}{\Gamma_{\mathrm{had}}} \cdot \mathrm{B}(b \to e)\, \varepsilon(b \to e) \\ & + 2 \cdot N_{\mathrm{had}} \cdot \frac{\Gamma_{b\bar{b}}}{\Gamma_{\mathrm{had}}} \cdot \mathrm{B}(b \to c \to e)\, \varepsilon(b \to c \to e) \\ & + 2 \cdot N_{\mathrm{had}} \cdot \frac{\Gamma_{b\bar{b}}}{\Gamma_{\mathrm{had}}} \cdot \mathrm{B}(b \to \tau \to e)\, \varepsilon(b \to \tau \to e) \\ & + 2 \cdot N_{\mathrm{had}} \cdot \frac{\Gamma_{c\bar{c}}}{\Gamma_{\mathrm{had}}} \cdot \mathrm{B}(c \to e)\, \varepsilon(c \to e), \end{aligned} \tag{3}$$

where N_{had} is the number of produced hadronic events, $2 \cdot N_{\mathrm{had}} \cdot \Gamma_{b\bar{b}}/\Gamma_{\mathrm{had}}$ is the number of b and $\bar{b}$ quarks produced, $\mathrm{B}(b \to e)$ is the average branching fraction of the types of b hadrons produced in Z^0 decay, and $\varepsilon(b \to e)$ is the acceptance for electrons from b hadron decays to satisfy the kinematic and geometric requirements $p > 4\,\mathrm{GeV/c}$, $p_t > 0.8\,\mathrm{GeV/c}$, and $|\cos\theta| < 0.7$. N^e_{prompt} has already been corrected for the efficiency of the electron identification criteria. The other terms are defined in an analogous way.

From this expression, we can determine the ratio of partial widths, $\Gamma_{b\bar{b}}/\Gamma_{\mathrm{had}}$:

$$\frac{\Gamma_{b\bar{b}}}{\Gamma_{\mathrm{had}}} = \frac{N^e_{\mathrm{prompt}} - N^e_c}{2 \cdot N_{\mathrm{had}} \cdot \Sigma(\mathrm{B} \cdot \varepsilon)}, \tag{4}$$

where N^e_c is the expected number of electrons from direct charm production (the last term in the above expression for N^e_{prompt}), $N_{\mathrm{had}} = 137\,600$ is the corrected number of hadronic events, and $\Sigma(\mathrm{B} \cdot \varepsilon)$ is the sum of the products of branching fractions times kinematic acceptances:

$$\begin{aligned} \Sigma(\mathrm{B} \cdot \varepsilon) = {} & \mathrm{B}(b \to e) \cdot \varepsilon(b \to e) \\ & + \mathrm{B}(b \to c \to e) \cdot \varepsilon(b \to c \to e) \\ & + \mathrm{B}(b \to \tau \to e) \cdot \varepsilon(b \to \tau \to e). \end{aligned} \tag{5}$$

The kinematic requirements $p > 4\,\mathrm{GeV/c}$ and $p_t > 0.8\,\mathrm{GeV/c}$ suppress the secondary decays so that the dominant term in $\Sigma(\mathrm{B} \cdot \varepsilon)$ (about 85%) is $\mathrm{B}(b \to e) \cdot \varepsilon(b \to e)$.

To determine $\Gamma_{b\bar{b}}/\Gamma_{\mathrm{had}}$, the kinematic acceptances are determined using a Monte Carlo simulation program, and the branching fractions are obtained from experimental measurements. Uncertainties in these branching fractions are the dominant systematic error in previous measurements of $\Gamma_{b\bar{b}}/\Gamma_{\mathrm{had}}$ [6–8]. For the values of $\mathrm{B}(b \to e)$ and $\mathrm{B}(b \to c \to e)$, we use the measurements [11] of $\mathrm{B}(b \to l\bar{\nu}_l X)$ and $\mathrm{B}(b \to c \to l\nu_l X)$ (with $l = e$ or μ) reported by the CLEO collaboration for the mixture of B^0_d and $B^{\pm}$ mesons produced at the $\Upsilon(4S)$ (only the CLEO collaboration reports a measurement of both $\mathrm{B}(b \to l\bar{\nu}_l X)$ and $\mathrm{B}(b \to c \to l\nu_l X)$). The branching fraction $\mathrm{B}(b \to l\bar{\nu}_l X)$ may not be the same at $\sqrt{s} \approx M_Z$, where presumably B^0_s and b baryons are produced, in addition to B^0_d and $B^{\pm}$. The sensitivity of our measurement to the assumption that it is the same is discussed below. We take into account expected differences in $\mathrm{B}(b \to c \to l\nu_l X)$ at $\sqrt{s} \approx M_Z$ and at the $\Upsilon(4S)$. Furthermore, although the statistical precision on $\mathrm{B}(b \to l\bar{\nu}_l X)$ is 2%, this branching fraction varies by more than 10% depending on which theoretical model of b hadron decay is used to extract $\mathrm{B}(b \to l\bar{\nu}_l X)$ from the data. This same model dependence, however, has the opposite effect on the acceptance, $\varepsilon(b \to e)$, and the branching fraction, $\mathrm{B}(b \to c \to l\nu_l X)$, so the sum of the products of the branching fractions times kinematic acceptances, $\Sigma(\mathrm{B} \cdot \varepsilon)$, exhibits reduced model dependence as will be shown below.

7.1 Branching fractions of b hadrons

To determine $\mathrm{B}(b \to l\bar{\nu}_l X)$ and $\mathrm{B}(b \to c \to l\nu_l X)$, the CLEO collaboration measures the momentum spectrum of electrons and muons. At the $\Upsilon(4S)$, the B mesons are very nearly at rest, so the lepton momentum in the laboratory is very close to the lepton momentum in the rest frame of the B-meson from which it originated. The leptons with momentum above 1.4 GeV/c come predominantly from $b \to l\bar{\nu}_l X$. Determining the branching fraction $\mathrm{B}(b \to l\bar{\nu}_l X)$ requires a model for the semileptonic decay spectrum of b hadrons to extrapolate to low momenta where the presence of secondary decays $b \to c \to l\nu_l X$ and experimental limitations in lepton identification preclude a direct measurement. Different models predict different extrapolations, which give different branching fractions.

The CLEO collaboration uses two models to extract the branching fraction. One is the spectator model of b hadron decay of Altarelli et al. [21] (ACM). The important parameters of this model, the mass of the charm quark and the Fermi momentum, are determined by fitting the measured lepton momentum spectrum. The second model is the form-factor model of Isgur et al. [22]

Table 4. The branching fractions of B mesons measured [11] at the $\Upsilon(4S)$ resonance by the CLEO collaboration. The three columns correspond to the three theoretical spectra used to extract the branching fractions from the data. The branching fractions $B(b\to l\bar{\nu}_l X)$ are the sum of $B(b\to c l\nu)$ and $B(b\to u l\nu)$

b hadron decay model	ISGW	ACM	ISGW**
$B(b\to l\bar{\nu}_l X)$ (%)	$9.9\pm0.1\pm0.4$	$10.5\pm0.2\pm0.4$	$11.2\pm0.3\pm0.4$
$B(b\to c\to l\nu_l X)$ (%)	$11.3\pm0.7\pm0.6$	$9.7\pm0.8\pm0.6$	$9.0\pm0.8\pm0.6$
$B(b\to u l\nu)$ (%)	$0.06\pm0.08\pm0.03$	$0.28+0.12\pm0.03$	$0.25\pm0.10\pm0.02$

(ISGW). This model determines the lepton spectrum from exclusive B meson three-body decays: $B\to Dl\nu$, $B\to D^*l\nu$, and $B\to D^{**}l\nu$; and it predicts the relative branching fractions of these three decay modes: 27%, 62%, and 11%, respectively. The CLEO collaboration also considers a variation of this model (ISGW**), in which the branching fraction of the $B\to D^{**}l\nu$ decay is treated as a free parameter determined by a fit to the lepton spectrum. The resulting relative branching fractions of $B\to Dl\nu$, $B\to D^*l\nu$, and $B\to D^{**}l\nu$ are 21%, 47%, and 32%. The branching fractions obtained using these three theoretical predictions of the lepton momentum spectrum are listed in Table 4. The fits of the three models to the data also determine the semileptonic branching fraction of B mesons with a $b\to u$ transition, instead of a $b\to c$ transition. These $B(b\to u l\nu)$ branching fractions are also listed in Table 4 and are in included in the calculation of the kinematic acceptances.

We assume that the value of $B(b\to l\bar{\nu}_l X)$ for the mix of b hadrons produced at $\sqrt{s}\approx M_Z$ is the same as the branching fraction measured at the $\Upsilon(4S)$. Under the reasonable assumption that the relative production rates of $B^{\pm}$ and B_d^0 are equal at both the $\Upsilon(4S)$ and at $\sqrt{s}\approx M_Z$, a difference between the semileptonic branching fractions of $B^{\pm}$ and B_d^0 [23] does not produce a difference between the average semileptonic branching fractions at the two energies. If, however, the semileptonic branching fractions of B_s^0 and b baryons are different from the average branching fractions of $B^{\pm}$ and B_d^0, the average semileptonic braching fraction at $\sqrt{s}\approx M_Z$ will be different from the value at the $\Upsilon(4S)$, where B_s^0 and b baryons are not produced. The values of the semileptonic branching fractions of B_s^0 and b baryons and the relative b hadron production rates are experimentally unknown; therefore, we have not attempted to include an estimate of the systematic error due to our assumption. Theoretical estimates [24] of the differences of semileptonic branching fractions between different b hadrons range from 10% to 30%. As an illustrative example, if the relative abundances of $B^{\pm}$, B_d^0, B_s^0, and Λ_b produced at $\sqrt{s}\approx M_Z$ are 40%, 40%, 12%, and 8% respectively, as given by the JETSET Monte Carlo, and the values of $B(B_s^0\to l\bar{\nu}_l X)$ and $B(\Lambda_b\to l\bar{\nu}_l X)$ are 20% smaller than the average semileptonic branching fraction of $B^{\pm}$ and B_d^0, then $B(b\to l\bar{\nu}_l X)$ would be 4.0% smaller at $\sqrt{s}\approx M_Z$ than at the $\Upsilon(4S)$. The resulting effect on $\Gamma_{b\bar{b}}/\Gamma_{\text{had}}$ is discussed at the end of this section when $\Sigma(B\cdot\varepsilon)$ is calculated.

Although we assume that the value of $B(b\to l\bar{\nu}_l X)$ is the same at $\sqrt{s}\approx M_Z$ and at the $\Upsilon(4S)$, the branching fraction $B(b\to c\to l\nu_l X)$ is expected to be different at $\sqrt{s}\approx M_Z$ due to the presence of B_s^0 and b baryons. We apply a correction factor to the branching fractions $B(b\to c\to l\nu_l X)$ given in Table 4 to take this difference into account. The contribution of $B(b\to c\to l\nu_l X)$ to $\Sigma(B\cdot\varepsilon)$ is relatively small, and $\Gamma_{b\bar{b}}$ as determined using (4) is much less sensitive to differences in this branching fraction at the two centre-of-mass energies than to differences in $B(b\to l\bar{\nu}_l X)$. The correction factor is calculated using the following experimental results and assumptions: the relative abundances of b hadrons at $\sqrt{s}\approx M_Z$ are as given above, the B_s^0 always decays to a D_s and b baryons always produce Λ_c; the relative semileptonic branching fractions of $D^{\pm}$, D^0, D_s, and Λ_c are the same as the fractions of the well-measured lifetimes [25] of these particles; and the abundances of these charmed particles from B meson decay at the $\Upsilon(4S)$ are the values measured by the CLEO collaboration [26]. The correction factor is 0.926. If the relative abundances of b hadrons produced at $\sqrt{s}\approx M_Z$ are changed to extreme values (equal amounts of $B^{\pm}$, B_d^0, and B_s^0, and 15% of the b hadrons produced are b baryons), this correction factor is 0.847. The assumptions that the B_s^0 always decays to D_s and b baryons always produce Λ_c are conservative; if these are not true, the value of the correction factor increases towards unity. In order to accommodate this value, the systematic error on the correction factor is taken to be 100% of the change:

- correction factor for $B(b\to c\to l\nu_l X)$ is 0.926 ± 0.074.

The branching fraction $B(b\to\tau\to e)$ is taken to be

- $B(b\to\tau\to e)=(0.044\pm0.018)\cdot B(b\to e)$.

The scaling factor above is the product of $B(b\to\tau)/B(b\to e)=0.25\pm0.10$ [27] and $B(\tau\to e)=0.177\pm0.004$ [25].

7.2 *Kinematic acceptances*

The kinematic acceptances are derived from a Monte Carlo simulation based on the JETSET program [18]. The simulation includes the effects of detector resolution on the jet finding and on the p and p_t measurements. In this Monte Carlo, there are four types of b hadrons that can decay semileptonically: B_d^0, $B^{\pm}$, B_s^0, and Λ_b; their relative abundance is 40%, 40%, 12%, and 8%, respec-

tively. The Λ_b hadron is produced with no preferred spin orientation. In the Monte Carlo simulation, the b quarks are hadronized using the Peterson fragmentation function [28] and have $\langle x_E \rangle_b = 0.72$, where $\langle x_E \rangle_b$ is the mean energy of the primary b hadrons divided by the beam energy. This value of $\langle x_E \rangle_b$ is consistent with OPAL published value $\langle x_E \rangle_b = 0.726 \pm 0.007 \pm 0.022$ [8], which is determined from a fit of the p and p_t spectrum of muons in hadronic events.

The value of the kinematic acceptance $\varepsilon(b \to e)$ determined using the JETSET Monte Carlo is 0.278 ± 0.003, where the error is due to Monte Carlo statistics. This acceptance includes a factor of 0.61 from the geometric requirement $|\cos\theta| < 0.7$, the efficiency for an electron to satisfy the requirements for a good track, and the efficiency for the event to have at least six good charged tracks.

In order to determine the dependence of the kinematic acceptance on the assumed form of the electron momentum spectrum we use the following procedure. For the decays of B_d^0 and $B^{\pm}$ mesons, the JETSET prediction of the momentum spectrum of the electron in the rest frame of the parent meson is reweighted so it agrees with the $b \to c l \nu$ spectra predicted by the different theoretical models of b hadron decay used by the CLEO collaboration to extract the branching fractions. The resulting corrections to the kinematic acceptance, $\varepsilon(b \to e)$, due to reweighting to the three different theoretical spectra are listed in Table 5. The same correction is applied for the decays of B_s^0 and b baryons. Effects on the momentum spectrum due to the possible polarization of b baryons are neglected. The kinematic acceptance is reduced by an additional 1.1% to account for the damping effect of radiative corrections [29] not included in the JETSET b hadron decays. The change due to this correction has been assigned a 100% systematic error. The Monte Carlo simulation does not include $b \to u l \nu$. Based on a comparison of the rest frame spectra of $b \to c l \nu$ and $b \to u l \nu$ predicted by the models, the kinematic acceptance for $b \to u l \nu$ semileptonic decays is taken to be a factor 1.5 larger than the kinematic acceptance of $b \to c l \nu$ decays. The kinematic acceptance is increased according to the measured fraction of $b \to u l \nu$ decays for each model. The resulting corrections for the three different theoretical spectra are given in Table 5. The changes due to the $b \to u$ corrections have been assigned a 100% systematic error. The final values of $\varepsilon(b \to e)$, corresponding to the three different theoretical spectra, after all corrections have been applied are summarized in Table 5.

Table 5. The kinematic acceptance calculated with the JETSET Monte Carlo [18] for an electron from b hadron semileptonic decay to satisfy $p > 4$ GeV/c, $p_t > 0.8$ GeV/c, and $|\cos\theta| < 0.7$, when the b hadrons are produced on the Z^0 resonance. The correction factors to this acceptance depend on which model of b hadron decay is used. The correction factors listed in the table are multiplicative and are explained in the text

$\varepsilon(b \to e)$ from JETSET	0.278		
b hadron decay model	ISGW	ACM	ISGW**
correction from reweighting	0.993	0.970	0.938
electroweak correction	0.989	0.989	0.989
correction for $b \to u$	1.003	1.013	1.011
corrected $\varepsilon(b \to e)$	0.274	0.270	0.261

The kinematic acceptances $\varepsilon(b \to c \to e)$ and $\varepsilon(b \to \tau \to e)$ are determined with the JETSET Monte Carlo:

- $\varepsilon(b \to c \to e) = 0.0490 \pm 0.0016$, and
- $\varepsilon(b \to \tau \to e) = 0.101 \pm 0.008$.

The errors are due to Monte Carlo statistics. The model dependent corrections that have been applied to $\varepsilon(b \to e)$ have not been applied to $\varepsilon(b \to c \to e)$ and $\varepsilon(b \to \tau \to e)$. This omission is expected to produce a systematic error of less than 1% in $\Gamma_{b\bar{b}}/\Gamma_{\text{had}}$.

7.3 *The charm contribution*

The number of electrons from direct charm production, $Z^0 \to c\bar{c}$, is given by

$$N_c^e = 2 \cdot N_{\text{had}} \cdot \frac{\Gamma_{c\bar{c}}}{\Gamma_{\text{had}}} \cdot \mathrm{B}(c \to e) \cdot \varepsilon(c \to e); \qquad (6)$$

where $\Gamma_{c\bar{c}}/\Gamma_{\text{had}}$ is taken to be the Standard Model value 0.171 [30] and $\mathrm{B}(c \to e)$ is taken to be equal to an average of measurements of $\mathrm{B}(c \to \mu) = 0.079 \pm 0.011$ [25]. The acceptance $\varepsilon(c \to e) = 0.0504 \pm 0.0031$ is determined by Monte Carlo simulation; the error is due to the Monte Carlo statistics. In the Monte Carlo simulation, the charm quarks are hadronized using the Peterson fragmentation function [28] and have $\langle x_E \rangle_c = 0.53$, consistent with the OPAL published value $\langle x_E \rangle_c = 0.56 \pm 0.02 \pm 0.03$ [8]. Using these numbers yields

- $N_c^e = 187 \pm 42$,

where the dominant contributions to the error are the 14% uncertainty on $\mathrm{B}(c \to e)$ and the 16% maximum variation from the value of $\varepsilon(c \to e)$ determined at $\langle x_E \rangle_c = 0.53$, when $\langle x_E \rangle_c$ is varied from 0.48 to 0.59.

7.4 *Calculating* $\Gamma_{b\bar{b}}/\Gamma_{\text{had}}$

The values of $\Sigma(\mathrm{B} \cdot \varepsilon)$ for the three different models are given in Table 6. When the branching fractions and kinematic acceptances specific to each model are used, $\Sigma(\mathrm{B} \cdot \varepsilon)$ shows only a small variation with the model that is considered. Using these values and the values of N^e_{prompt}, N_{had}, and N_c^e given above, we determine the values of $\Gamma_{b\bar{b}}/\Gamma_{\text{had}}$ given in Table 6. The error on $\Gamma_{b\bar{b}}/\Gamma_{\text{had}}$ is the experimental statistical error on N^e_{prompt}. The systematic errors are summarized in the next section. For our final number of $\Gamma_{b\bar{b}}/\Gamma_{\text{had}}$, we quote the value obtained using the ACM model. The variation of this value of $\Gamma_{b\bar{b}}/\Gamma_{\text{had}}$ with the values obtained with the two other models is included as a systematic error.

Returning to our illustrative example, if $\mathrm{B}(b \to l \bar{\nu}_l X)$ were 4.0% smaller at $\sqrt{s} \approx M_Z$ than at the $\Upsilon(4S)$, the

Table 6. The composition and values of $\Sigma(B\cdot\varepsilon)$ for the three different models of b hadron decay, and the corresponding values of $\Gamma_{b\bar{b}}/\Gamma_{had}$. The error is the statistical error on N^e_{prompt}

b hadron decay model	ISGW	ACM	ISGW**
$B(b\to e)\cdot\varepsilon(b\to e)$	0.0271	0.0284	0.0292
$B(b\to c\to e)\cdot\varepsilon(b\to c\to e)$	0.0051	0.0044	0.0041
$B(b\to\tau\to e)\cdot\varepsilon(b\to\tau\to e)$	0.0004	0.0005	0.0005
$\Sigma(B\cdot\varepsilon)$	0.0327	0.0332	0.0338
$\Gamma_{b\bar{b}}/\Gamma_{had}$	0.230 ± 0.008	0.226 ± 0.008	0.223 ± 0.008

value of $\Sigma(B\cdot\varepsilon)$ in the ACM model would decrease by 3.4% with a corresponding increase in $\Gamma_{b\bar{b}}/\Gamma_{had}$ as determined using (4).

8 Systematic errors

The systematic errors due to the hadronic event selection, the electron identification efficiency, the contamination from photon conversions, the knowledge of the hadronic background, the direct charm contribution, the uncertainty in the radiative corrections in the decay, and b hadron decay model dependence have already been discussed. These contributions to the total systematic error are listed in Table 7. The 4.0% and 1.1% systematic errors on N^e_{prompt}, due to the uncertainties in the electron identification efficiency and hadronic background respectively, result in 4.4% and 1.2% systematic errors on $\Gamma_{b\bar{b}}/\Gamma_{had}$ after the number of electrons from direct charm production has been subtracted. Further sources of systematic error are discussed below.

The sensitivity of $\Gamma_{b\bar{b}}/\Gamma_{had}$ to the b quark fragmentation has been assessed by varying $\langle x_E\rangle_b$ from 0.68 to 0.76. This variation changes $\varepsilon(b\to e)$, $\varepsilon(b\to c\to e)$, and $\varepsilon(b\to\tau\to e)$ simultaneously. When $\langle x_E\rangle_b$ is varied in this range, the maximum variation in $\Gamma_{b\bar{b}}/\Gamma_{had}$ from the above central value is 3.0%.

Table 7. Summary of the systematic errors considered in the determination of $\Gamma_{b\bar{b}}/\Gamma_{had}$. The individual systematic errors are added in quadrature resulting in a total systematic error of 8.0% on the measured value of $\Gamma_{b\bar{b}}/\Gamma_{had}$

Systematic error source	% of measurement
hadronic event selection	0.4%
electron identification efficiency	4.4%
photon conversion subtraction	2.8%
knowledge of hadronic background	1.2%
direct charm contribution	2.0%
radiative corrections in decay	1.0%
model variation of B decay	1.7%
fragmentation of b quarks	3.0%
CLEO errors on $B(b\to l\bar{\nu}_l X)$ and $B(b\to c\to l\nu_l X)$	3.9%
Monte Carlo statistics in ε	1.1%
correction to $\varepsilon(b\to e)$ from $b\to u$	1.1%
correction to $B(b\to c\to l\nu_l X)$	1.0%
uncertainty in $B(b\to\tau\to e)$	0.6%
Total systematic uncertainty	8.0%

The systematic error due to the experimental errors on the measurements of $B(b\to l\bar{\nu}_l X)$ and $B(b\to c\to l\nu_l X)$ (the errors given in Table 4) is 3.9%. In calculating this error on $\Gamma_{b\bar{b}}/\Gamma_{had}$, we have assumed that the errors on $B(b\to l\bar{\nu}_l X)$ are uncorrelated with the errors on $B(b\to c\to l\nu_l X)$.

The systematic error in $\varepsilon(b\to e)$, $\varepsilon(b\to c\to e)$, and $\varepsilon(b\to\tau\to e)$ due to Monte Carlo statistics is 1.1%. The systematic error due to the uncertainty in the correction to $\varepsilon(b\to e)$ that accounts for $b\to u$ decays is 1.1%. The systematic error due to the uncertainty in the correction to $B(b\to c\to l\nu_l X)$ that accounts for the presence of B^0_s and Λ_b is 1.0%. The systematic error due to the uncertainty in $B(b\to\tau\to e)$ is 0.6%.

The final value for $\Gamma_{b\bar{b}}/\Gamma_{had}$ is

$$\Gamma_{b\bar{b}}/\Gamma_{had}=0.226\pm0.008\pm0.018,$$

where the first error is statistical and the second is systematic.

As an additional check on the result, the minimum momentum of electron candidates was reduced to 2 GeV/c. The number of electron candidates found with $2<p<4$ GeV/c is 356. The estimated background from photon conversions is 114 ± 29, and the measured hadronic background is 4 ± 1. The resulting additional signal is $238\pm17\pm29$, where the first error is statistical and the second error is due to the uncertainty in the background from photon conversions. The identification efficiency in this momentum bin is 0.463 ± 0.028. The value of $\Gamma_{b\bar{b}}/\Gamma_{had}$ obtained if these additional electrons are included is $0.230\pm0.007\pm0.019$. This value is in good agreement with the value obtained for $p>4$ GeV/c; the difference between the two results is within the expected fluctuation due to the additional statistics. Reducing the momentum cut slightly reduces the correction of the JETSET kinematic acceptance, $\varepsilon(b\to e)$, and reduces the uncertainties due to the c quark and b quark fragmentation. On the other hand, the increased background from photon conversions substantially increases the systematic error due to this source.

The number of prompt electrons can also be used to determine the product

$$\frac{\Gamma_{b\bar{b}}}{\Gamma_{had}}\cdot B(b\to e^-\bar{\nu}_e X)=0.0238\pm0.0008\pm0.0020,$$

where the first error is statistical and the second is systematic. The product has been determined using the ACM

model; the uncertainty due to modelling contributes 0.0011 to the systematic error. The modelling uncertainty contributes a systematic error of 4.7% on the product compared to a systematic error of 1.7% on $\Gamma_{b\bar{b}}/\Gamma_{\text{had}}$.

9 Discussion and conclusion

Using the value of $\Gamma_{\text{had}} = 1739 \pm 17$ MeV measured by the OPAL collaboration [1], the value of $\Gamma_{b\bar{b}}$ is

$$\Gamma_{b\bar{b}} = 394 \pm 13 \pm 32 \text{ MeV},$$

where the first error is statistical and the second is systematic. We have assumed that the average semileptonic branching fraction of B mesons produced at the $\Upsilon(4S)$ is the same as the average semileptonic branching fraction of b hadrons produced at $\sqrt{s} \approx M_Z$. This measured value agrees within errors with the value predicted by the Standard Model of 378 MeV [30]. Because this measurement depends on the region of the lepton momentum spectrum that is dominated by $b \to l\bar{\nu}_l X$ at the $\Upsilon(4S)$, only a small error is introduced due to the uncertainties in the model of B meson decay. The largest experimental component of the systematic error is the uncertainty in the electron identification efficiency. This uncertainty is dominated by the statistical precision with which the efficiency has been measured.

An alternative to assuming that the effective semileptonic branching fraction of b hadrons at $\sqrt{s} \approx M_Z$ is the same as the semileptonic branching fraction of B mesons at the $\Upsilon(4S)$ is to use the average value of $\text{B}(b \to l\bar{\nu}_l X)$ from measurements at PEP and PETRA. While the composition of b hadrons produced at these colliders is expected to be similar to the composition at $\sqrt{s} \approx M_Z$, these measurements are difficult to interpret. This is because the sensitivity of these measurements to which model of b hadron decay used to extract $\text{B}(b \to l\bar{\nu}_l X)$ has not been reported. The uncertainty should be at least as large as the uncertainty found by the CLEO collaboration. The L3 collaboration has measured [7] $\text{B}(b \to l\bar{\nu}_l X)$ using the ratio of the number of hadronic events with two identified leptons to the number of leptons in hadronic events. The statistical precision of this measurement is 9%.

Our assumption that all b hadrons have similar semileptonic branching fractions may soon be tested by measurements of the lifetimes of B_s^0 and Λ_b, which are expected to be proportional to their semileptonic branching fraction. If, as expected, B_s^0 and b baryons are about 20% of the mixture of b hadrons produced at $\sqrt{s} \approx M_Z$, lifetime measurements with a precision of 5% would contribute an error of about 1% to $\Gamma_{b\bar{b}}$.

In conclusion, by measuring the production rate of electrons with large momentum and large momentum transverse to the nearest jet, we have determined $\Gamma_{b\bar{b}}$ using a procedure that reduces the dependence of the result on the model of semileptonic b hadron decay considered.

Acknowledgements. We would like to thank colleagues in the CLEO collaboration for supplying computer programs and detailed data necessary for the reweighting of our simulated electron momentum spectrum to the various theoretical models of b hadron decay. It is also a pleasure to thank the SL Division for the efficient operation of the LEP accelerator and their continuing close cooperation with our experimental group. In addition to the support staff at our own institutions we are pleased to acknowledge the Department of Energy, USA; National Science Foundation, USA; Science and Engineering Research Council, UK; Natural Sciences and Engineering Research Council, Canada; Israeli Ministry of Science; Minerva Gesellschaft; Japanese Ministry of Education, Science and Culture (the Monbusho) and a grant under the Monbusho International Science Research Program; American Israeli Bi-national Science Foundation; Direction des Sciences de la Matière du Commissariat à l'Energie Atomique, France; Bundesministerium für Forschung und Technologie, FRG; A.P. Sloan Foundation and Junta Nacional de Investigação Científica e Tecnológica, Portugal.

References

1. OPAL Coll., G. Alexander et al.: Z. Phys. C - Particles and Fields 52 (1991) 175
2. A.A. Akhundov, D. Yu. Bardin, T. Riemann: Nucl. Phys. B276 (1986) 1; J. Bernabéu, A. Pich, A. Santamaría: Phys. Lett. B200 (1988) 569; W. Beenakker, W. Hollik: Z. Phys. C - Particles and Fields 40 (1988) 141; B.W. Lynn, R.G. Stuart: Phys. Lett. B252 (1990) 676
3. P. Langacker, D. London: Phys. Rev. D38 (1988) 886
4. The deviations from the Standard Model depend on the mixing angle between the ordinary and exotic fermions, and limits on these mixing angles based on LEP data have been published: E. Nardi, E. Roulet: Phys. Lett. B248 (1990) 139; E. Nardi, E. Roulet, D. Tommasini: Global analysis of fermion mixing with exotics, FERMILAB PUB-91/207-A
5. MARK II Coll., J.F. Kral et al.: Phys. Rev. Lett. 64 (1990) 1211
6. ALEPH Coll., D. Decamp et al.: Phys. Lett. B244 (1990) 623
7. L3 Coll., B. Adeva et al.: Phys. Lett. B241 (1990) 416; L3 Coll., B. Adeva et al.: Phys. Lett. B261 (1991) 177
8. OPAL coll., M.Z. Akrawy et al.: Phys. Lett. B263 (1991) 311
9. MARK II Coll., R.G. Jacobsen et al.: Phys. Rev. Lett. 67 (1991) 3347
10. DELPHI Coll., P. Abreu et al.: Z. Phys. C - Particles and Fields 53 (1992) 567; DELPHI Coll., P. Abreu et al.: Phys. Lett. B281 (1992) 383
11. CLEO Coll., S. Henderson et al.: Phys. Rev. D45 (1992) 2212; M. Worris: Thesis, Cornell University, 1991
12. Crystal Ball Coll., K. Wachs et al.: Z. Phys. C - Particles and Fields 42 (1989) 33; ARGUS Coll., H. Albrecht et al.: Phys. Lett. B249 (1990) 359; CUSB Coll., C. Yanagisawa et al.: Phys. Rev. Lett. 66 (1991) 2436
13. OPAL Coll., K. Ahmet et al.: Nucl. Instrum. Methods A305 (1991) 275
14. M. Hauschild et al.: Nucl. Instrum. Methods A314 (1992) 74 Instrum. Methods
15. W. Bartel et al.: Z. Phys. C - Particles and Fields 33 (1986) 23; S. Bethke et al.: Phys. Lett. B213 (1988) 235
16. OPAL Coll., M.Z. Akrawy et al.: Z. Phys. C - Particles and Fields 49 (1991) 375
17. OPAL Coll., M.Z. Akrawy et al.: Z. Phys. C - Particles and Fields 50 (1991) 373
18. T. Sjöstrand: Comput. Phys. Comm. 39 (1986) 347; we used version 7.2 of the JETSET program with parameters tuned to the OPAL data as described in: OPAL Coll., M.Z. Akrawy et al.: Z. Phys. C - Particles and Fields 47 (1990) 505
19. J. Allison et al.: CERN-PPE/91-234, submitted to Nucl. Instrum. Methods
20. OPAL Coll., G. Alexander et al.: Phys. Lett. B264 (1991) 219
21. G. Altarelli et al.: Nucl. Phys. B208 (1982) 365; the values of the parameters in the ACM model are the mass of the charm

quark $m_c = 1673\ \mathrm{MeV/c^2}$ and the Fermi momentum $p_f = 298\ \mathrm{MeV/c}$
22. N. Isgur, D. Scora, B. Grinstein, M.B. Wise: Phys. Rev. D39 (1989) 799
23. The ratio of the semileptonic branching fractions of $B^{\pm}$ and B_d^0 is expected to be the same as the ratio of their lifetimes. The ratio of lifetimes $\tau(B^{\pm})/\tau(B_d^0)$ has been determined to be $1.00 \pm 0.23 \pm 0.14$ from measurements made by ARGUS Coll., H. Albrecht et al.: Phys. Lett. B232 (1989) 554, and $0.89 \pm 0.19 \pm 0.13$ from measurements made by the CLEO coll., R. Fulton et al.: Phys. Rev. D43 (1991) 651, under the assumption that equal numbers of charged and neutral B mesons are produced at the $\Upsilon(4S)$
24. G. Altarelli, S. Petrarca: Phys. Lett. B261 (1991) 303; I.I. Bigi: Phys. Lett. B169 (1986) 101; J.H. Kühn et al.: Heavy flavours at LEP, MPI-PAE/PTh 49/89, 1989, contribution by R. Rückl, p. 59; M.A. Schiffman: Proc. of the 1987 int. symp. on lepton and photon interactions at high energies, Hamburg 1987, Nucl. Phys. B (Proc. Suppl.) 3 (1988) 289
25. J.J. Hernandez et al.: Particle Data: Phys. Lett. B239 (1990) 1
26. CLEO Coll., D. Bortoletto et al.: Phys. Rev. D45 (1992) 21 Phys. Rev. D
27. C. Quigg, J.L. Rosner: Phys. Rev. D19 (1979) 1532. We use the phase space formulas given in this paper with $m_b = 5.0\ \mathrm{GeV/c^2}$ and $m_c = 1.5\ \mathrm{GeV/c^2}$. The error on this number comes from varying these mass values between the following limits: $4.8 < m_b < 5.2\ \mathrm{GeV/c^2}$ and $1.2 < m_c < 1.8\ \mathrm{GeV/c^2}$
28. C. Peterson et al.: Phys. Rev. D27 (1983) 105
29. D. Atwood, W.J. Marciano: Phys. Rev. D41 (1990) 1736
30. This is the Standard Model prediction calculated using the lineshape program ZFITTER, Dubna-Zeuthen radiative correction group (based on the ZBIZON package): D.Yu. Bardin et al.: Berlin-Zeuthen preprint 89-08, 1989; R. Kleiss et al., in: Z. Physics at LEP1, CERN Yellow report 89-08, ed. G. Altarelli et al., Vol. 3, 1989. For this prediction, the Z^0, top quark, and Higgs boson masses are $M_Z = 91.17\ \mathrm{GeV/c^2}$, $M_{\mathrm{top}} = 130\ \mathrm{GeV/c^2}$, and $M_{\mathrm{Higgs}} = 100\ \mathrm{GeV/c^2}$